Optical Metrology of Thin Films

by

Randy Logan

B.S.E. Materials Science and Engineering
University of Michigan, 1994

Submitted to the Department of Materials Science and Engineering in Partial Fulfillment of the Requirements for the Degree of

Master of Science in Materials Science and Engineering

at the

Massachusetts Institute of Technology

June, 1997

Signature of Author.....
Department of Materials Science and Engineering
May 9, 1997

Certified by.....
Keith A. Nelson
Department of Chemistry
Thesis Supervisor

Certified by.....
Carl Thompson
Department of Materials Science and Engineering
Thesis Reader

Accepted by.....
Linn Hobbs
John F. Elliot Professor of Materials
Chairman, Department Committee on Graduate Students

Science

Optical Metrology of Thin Films

by

Randy Logan

Submitted to the Department of Materials Science and Engineering
in Partial Fulfillment of the Requirements for the Degree of Master of
Science Department of Materials Science and Engineering

Abstract

A non-contact and non-destructive laser-based acoustic technique called impulsive stimulated thermal scattering (ISTS) is demonstrated for new applications in the context of a compact, portable apparatus. ISTS is used to determine viscoelastic and thermal transport properties of a DuPont Kapton film before and after neutron irradiation to determine the changes that would be expected to occur in a nuclear reactor environment. The results demonstrate general capabilities for *in-situ,* non-destructive evaluation (NDE) of radiation-induced material degradation. The specific application demonstrated is evaluation of insulation materials to be used in a superconducting magnet design in the International Thermonuclear Experimental Reactor (ITER). ISTS is also used to measure thicknesses of metal films in single-layer and multilayer assemblies such as W/Si, Al/Si, and Al/W/Si. Thicknesses are determined to a precision of less than ± 100 Angstroms for submicron films. ISTS and conventional measurements (profilometry, X-ray fluorescence, scanning electron microscopy, and 4-point resistance) are made on the same samples and the results are found to compare favorably. Measurements are demonstrated with a laboratory version of the apparatus, using conventional large-frame lasers and optics, and in a commercial prototype using compact diode-pumped and diode lasers and optics which all fit onto a 1-ft x 2-ft breadboard.

Thesis Supervisor: Keith A. Nelson
Thesis Reader: Carl Thompson

Table of Contents

List of Figures

List of Tables

Acknowledgments

I would like to acknowledge, first and foremost, my advisor Keith Nelson for giving me the opportunity to participate in this project and to interact with the entrepreneurial side of his work. Keith helped me make the transition from Materials Science Engineering into Chemistry fairly straightforward by focusing me on the applications end of picosecond ultrasonics. I would like to thank Alex Maznev for patiently teaching me about lasers, optics and sound waves in materials and all other members of the Nelson research group for their help. I give a big thank you to Active Impulse Systems, Inc. for allowing me to participate in the startup effort in many ways and learn what it takes to launch a high-tech company. Specifically, I thank Matt Banet for spending a lot of time teaching me about the technique and guiding my research efforts, Martin Fuchs for teaching me product development, John Hanselman for showing me the links between technology and business and John Rogers for insightful discussions and data analysis help. Lastly, I would like to thank my very soon to be wife, Ann, and my parents, Ron and Karen, for supporting me throughout my stay at MIT.

This work was supported in part by NSF Grant no. DMR-9317198 and by the MIT Lincoln Laboratory Advanced Concepts Program, principally sponsored by the Dept. of the Air Force. R.L. acknowledges an NSF Graduate Fellowship.

Chapter 1: Introduction

Thin films comprise a rapidly advancing area of technology and play integral roles in devices used in the microelectronics, biotechnology, automotive and aerospace industries. Much effort is spent tailoring material properties in thin films to achieve critical performance criteria under operating conditions. The need to characterize these material properties for widely varying applications has spurred the growth of many new characterization methods and instruments. Unfortunately, many of these techniques are destructive in nature and do not provide information about the material under its operating conditions. The ideal characterization method would provide information on material properties under operating conditions without requiring destructive sectioning. Such techniques fall under the category of non-destructive evaluation [1,2].

Non-destructive evaluation techniques rely on many different methods such as elastic waves, penetrating radiation, light, electric and magnetic fields, chemical sensing, etc. Often the properties critical to thin film performance include the mechanical, thermal and physical properties of the film. Ultrasonic NDE is used to characterize these properties by introducing low-level high frequency stress waves into the material being examined. Ultrasonic, or acoustic, waves propagate according to the mechanical and physical conditions present in the material and are detected and interpreted to give the needed information [1-4].

As new thin film materials, applications and processes are developed, there is a growing need to characterize the properties of these thin films, both in a research environment with new technologies and in a manufacturing environment with process control instruments. The motivation behind this research is the transfer of one such ultrasonic thin film characterization technology out of an academic research environment and into industry.

Over the last decade, many advances have been made in the area of picosecond ultrasonics in the Nelson research group at MIT. One technique, impulsive stimulated thermal scattering (ISTS), is an all optical method of exciting and detecting acoustic waveguide modes in thin films. With this technique, many properties of several categories of thin film materials have been analyzed. ISTS has been used for determination of thin film elastic moduli [3-8], thermal diffusivities [5,6,8], residual stress [9], delamination from substrates [10], and structural evolution during cure [11].

Through collaborations with Mordechai Rosthchild at MIT Lincoln Laboratories on a project involving the use of ISTS to examine packaging materials for microelectronic products, a potential commercial application of ISTS was identified. The microelectronics industry is very dependent on thin film technology. The success of a semiconductor device is extremely sensitive to the quality and uniformity of the films fabricated in the manufacturing environment. As tolerances become tighter and wafer sizes become larger, quality control becomes an increasingly important problem. Good process control throughout the 100 or more steps required to make a semiconductor device is critically important to being able to profitably make a product. One area of process control that currently requires relatively destructive and non-value added metrology is metal film thickness. Metal films are used throughout integrated circuit (IC) fabrication as diffusion barriers, electrical contacts and adhesion promoters. Thickness variations can alter a film's mechanical and electrical properties, thereby affecting the performance of the circuit.

The awareness of a need for metal film thickness metrology in semiconductor manufacturing combined with the recent advent of compact, solid-state lasers with suitable performance characteristics for ISTS laid the foundation for the commercialization of ISTS as a thin-film metrology instrument for the microelectronics industry. This thesis will focus on the application of ISTS as a thin-film thickness characterization technique and the development of a compact prototype instrument. In parallel with the efforts to move ISTS into the

microelectronics industry, research efforts have been continuing on other fronts as well and will also be described in this thesis.

Chapter 2: Background

Impulsive Stimulated Thermal Scattering (ISTS), is an all-optical, non-contact, non-destructive technique [12]. In ISTS, two laser beams containing optical pulses each having a duration of a few hundred picoseconds are temporally and spatially overlapped at a sample's surface. Optical interference between the crossed beams forms a spatially varying interference or "grating" pattern of alternating light (constructive interference) and dark (destructive interference) regions, characterized by fringe spacing Λ or wavevector (here taken to be a scalar) $q = 2\pi/\Lambda = \lambda/2\sin(\theta/2)$ where λ and θ are respectively the wavelength of and angle between the excitation pulses. The light and dark regions are the grating "peaks" and "nulls" shown in figure 1. The sample absorbs radiation in the light regions, resulting in a mild heating and thermal expansion that launches coherent acoustic waves whose wavelength and direction match those of the interference pattern. The acoustic waves generate a time-dependent "ripple" on the sample's surface, as shown in figure 2. The ripple has a depth of modulation that oscillates at the acoustic frequency, which in turn is determined by the sample's mechanical (i.e. elastic) and physical (i.e. thickness) properties and by the boundary conditions (i.e. adhesion) between the different layers in the sample. After the acoustic waves are fully damped, heat flows from the heated grating peaks to the unheated grating nulls at a rate determined by the sample's thermal diffusivity.

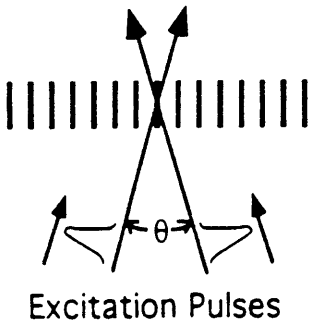

Figure 1: Two excitation pulses cross at angle, θ, creating an interference, or "grating" pattern.

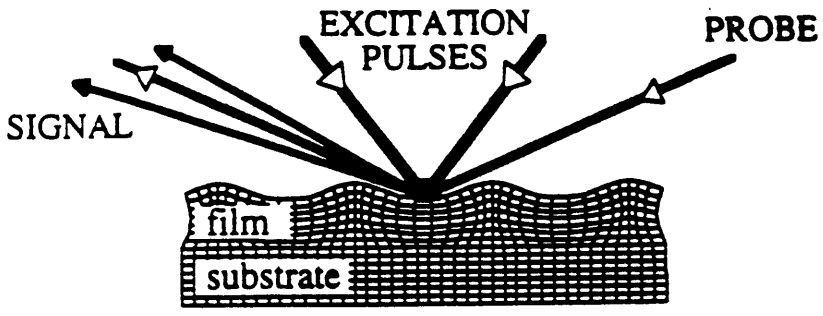

Figure 2: Surface "ripple" created by impulsive heating in a grating pattern. Probe beam is shown diffracting off from the grating created by the ripple.

The entire acoustic response is measured by diffracting a continuous probe laser beam off the surface ripple. This forms a signal beam which is then detected with a high-bandwidth photodetector to generate a light-induced signal waveform. Figure 3a shows a representative signal waveform measured from a thin titanium film which was electron beam deposited on a silicon substrate with a thermally grown 5000-A oxide layer. The data shown are the average of 200 single-laser-shot data scans and were collected in less than 5 seconds. The grating wavevector was 6.52 μm in this example. During the first few hundred nanoseconds, the signal waveform oscillates and decays according to the acoustic frequency and damping rate of the aluminum film. The inset shows the slower, non-oscillatory decay over the first 100 nanoseconds, which is due to thermal diffusion in the sample. Figure 3b shows the fourier transform of the data, revealing that the frequency of the oscillations is 612 MHz. From the acoustic information provided through ISTS, sound velocities and film thicknesses can be determined. From ISTS measurements made at several acoustic wavevectors, the acoustic dispersion relations and film elastic moduli can also be deduced. Based on the bulk titanium elastic moduli and density values, our result yields a film thickness of 1844 ± 20A for the data shown in figure 3a. Figures 3c and 3d show representative data scan from aluminum and titanium:nitride films with frequency domain data plotted in the inset.

The theory for acoustic mode propagation in thin films is well known and is presented elsewhere [13-15]. A film acts as an acoustic waveguide, supporting acoustic waveguide modes whose displacements include both shear and compression. Each waveguide mode has a characteristic dispersion relation giving the acoustic velocity v as a function of the wavevector q. Most important for thin film thickness determination is the fact that the acoustic velocity of each waveguide mode has the same dependence on the wavevector q and the film thickness d, so that if the product qd, i.e. the ratio of the acoustic wavelength Λ to the film thickness d, is held constant then the acoustic velocity is invariant. In practice, this means that if the dispersion

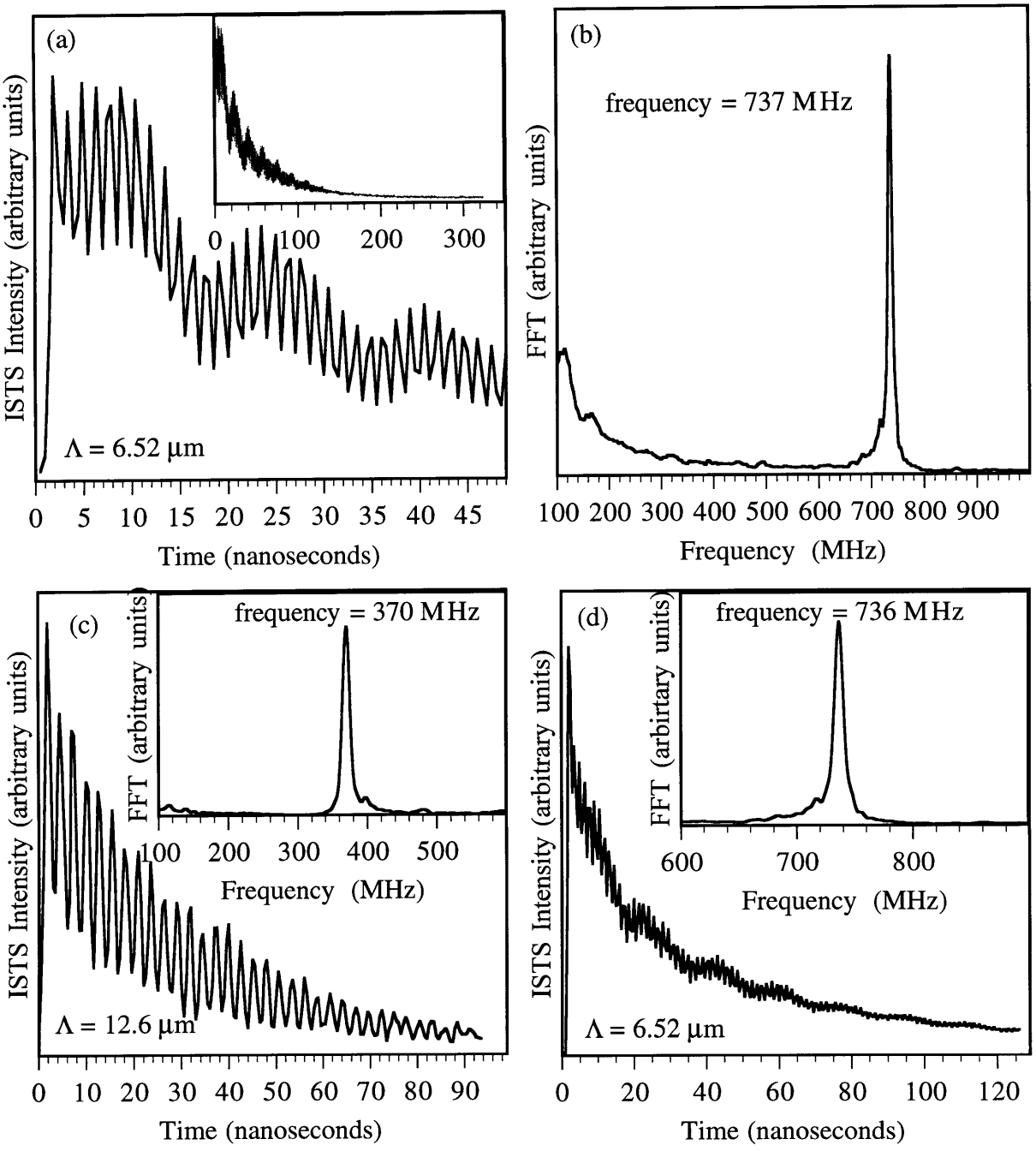

Figure 3: (a) ISTS Signal from 1800-A Ti on 5000-A oxide on silicon. Inset shows data on longer time scale to illustrate thermal diffusion. (b) Power spectrum of data in (a) showing frequency of 737 MHz. (c) ISTS signal from 8500-A Al on 5000-A oxide on silicon. Inset shows power spectrum (370 MHz). (d) ISTS signal on 1000-A TiN on oxide on silicon. Inset shows power spectrum (736 MHz). Note wavevector that data scans were collected at (Λ).

relation for the film (determined by the elastic modulus and density of the film and the underlying substrate) is known, and the ISTS grating wavevector is measured, then through measurement of the acoustic frequency, the acoustic velocity and the film thickness can be determined. Figure 4 shows a dispersion relationship (acoustic velocity versus the product, *qd*) calculated for a tungsten film on silicon. Fixing the thickness at a specific value, an expression for the sensitivity of the frequency to small changes in thickness as a function of wavevector can be derived:

$$f = \frac{q \cdot v(qd)}{2\pi}$$

$$\frac{\partial f}{\partial d} = \frac{q^2}{2\pi} \cdot \frac{\partial v(qd)}{\partial d} = \frac{(qd)^2}{2\pi d^2} \cdot \frac{\partial v(qd)}{\partial d}$$

Applying this equation to a 10,000-A tungsten film on silicon results in the sensitivity curve seen in figure 5. The x-axis goes out to q = 4 μm^{-1} to show the parabolic behavior of the sensitivity. In practice, the upper limit on the wavevector is defined by the bandwidth of the system. At wavevectors much larger than 2 μm^{-1}, the frequencies excited in thin metal films on silicon go above 1 GHz and are not detected by the detection system. For this example, the maximum attainable sensitivity of ISTS to changes in thickness is 0.04 MHz/A. If a 1 MHz frequency resolution is achievable, then the resolution of the technique should theoretically be 25 A. This result assumes that there is no change in mechanical properties of the film or the substrate from one sample to the next or across different regions of a sample.

In practice, as the film becomes thinner, its acoustic response is influenced to a greater extent by the properties of the underlying layers. For example, an acoustic wave excited in a metal film propagates through a proportionately larger amount of an underlying silicon substrate as the thickness of the metal film decreases. Because the silicon substrate is stiffer than the metal film, the frequency of the acoustic wave increases. Conversely, a thicker metal film takes

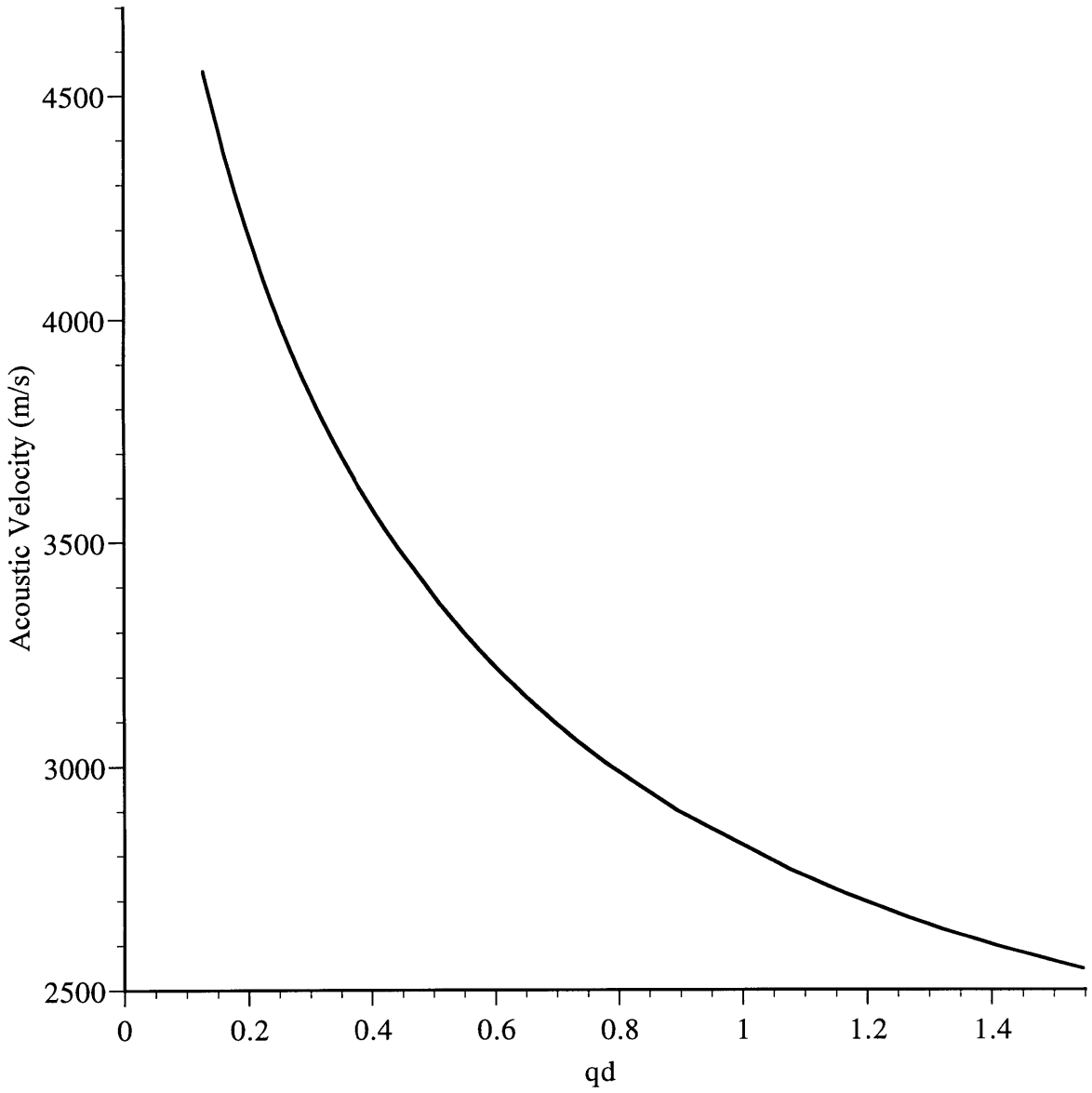

Figure 4: Dispersion relationship for tungsten on silicon. Parameters are: tungsten longitudinal velocity = 5220 m/s, tungsten transverse velocity = 2159 m/s, tungsten density = 17.42 g/cc, silicon longitudinal velocity = 9000 m/s, silicon transverse velocity = 5588 m/s, silicon density = 2.33 g/cc.

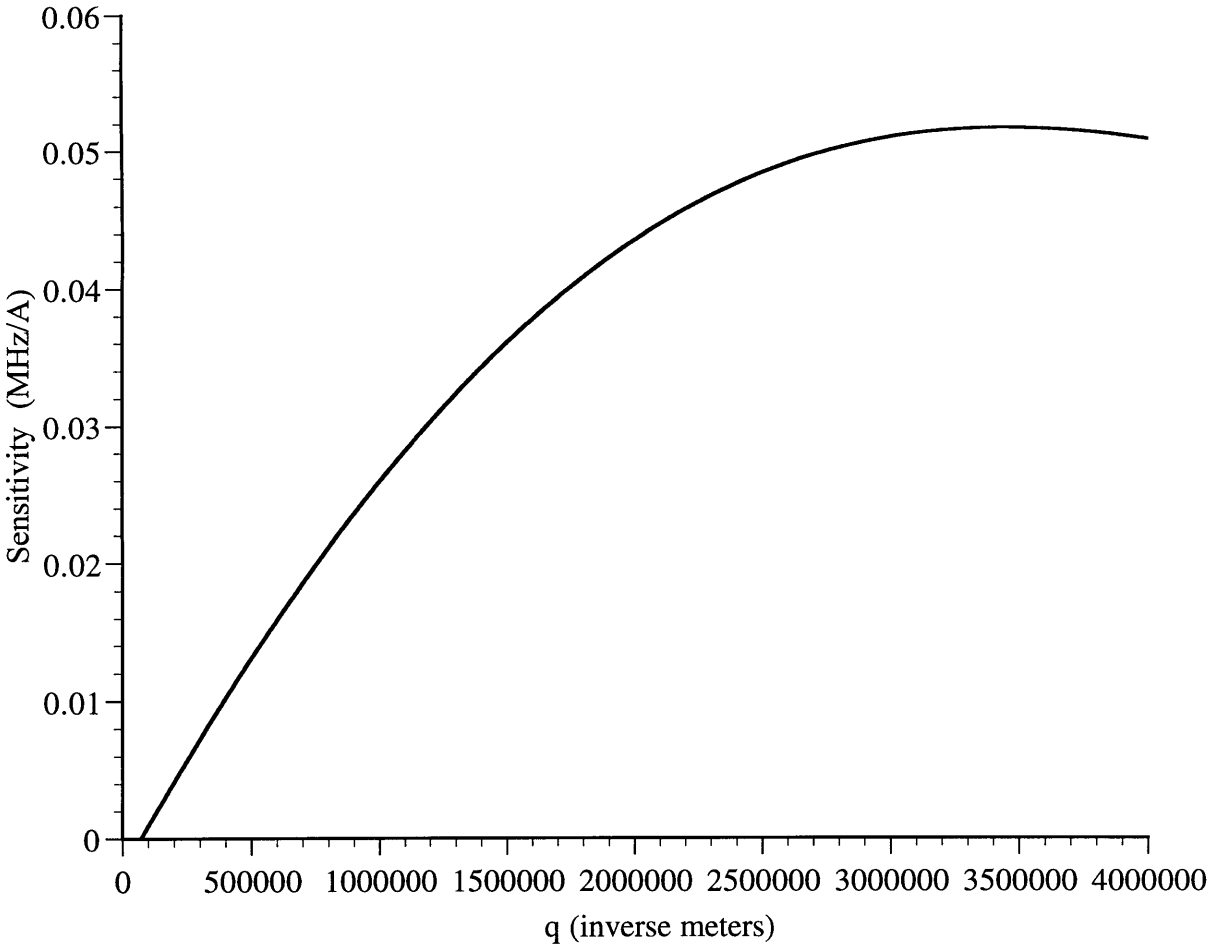

Figure 5: Sensitivity of ISTS frequency to thickness changes as a function of wavevector for a 5000-A tungsten film on silicon. The practical limit on q is approximately 2,000,000 m^{-1}.

on proportionately less of the acoustic properties of the underlying silicon, and therefore supports a lower frequency acoustic wave. This phenomenon is clearly demonstrated in figure 6 which shows ISTS measurements at a single wavevector (Λ=8μm) of varying thicknesses of titanium on silicon. The vertical lines are drawn to show that the frequency is changing a small amount as the film thickness changes. The lines depict the start and end of 45 oscillations in each case. The figure also shows the effect that changing the film thickness has on the signal level, with the signal level decreasing with thickness. This behavior is material dependent and has been found to be the opposite in Ti:N.

The dependence of the acoustic frequency on the wavevector is illustrated in figure 7. Here, a single film (2000-A titanium on silicon) has been probed at 4 different wavevectors and the acoustic frequency is seen to increase as the wavevector increases (or acoustic wavelength decreases). Figure 7 also demonstrates the effect of different wavevector has on the signal level. In the case of most metals, the signal level decreases with higher acoustic frequencies. Also, data taken at higher acoustic frequencies usually damps away faster but this phenomenon is not apparent in titanium because of its unusually low damping characteristics.

In addition to film thickness, the signal collected contains information on the thermal properties and stiffness of the film. For the purpose of determining film thickness, this data has no real value. For some other projects being pursued, however, this data contains valuable information. In the same manner that changes in acoustic frequency indicate changes in film thickness, changes in acoustic frequency also indicate changes in stiffness properties, changes in thermal decay rate indicate changes in thermal diffusivity and changes in acoustic damping contain information on loss moduli. No extensive quantitative interpretation of these properties is discussed and hence the theory presented on these properties will be brief.

In ISTS, the film absorbs heat in the spatially periodic pattern defined by the wavevector. Sudden spatially periodic heating causes the material to expand where light was incident. After

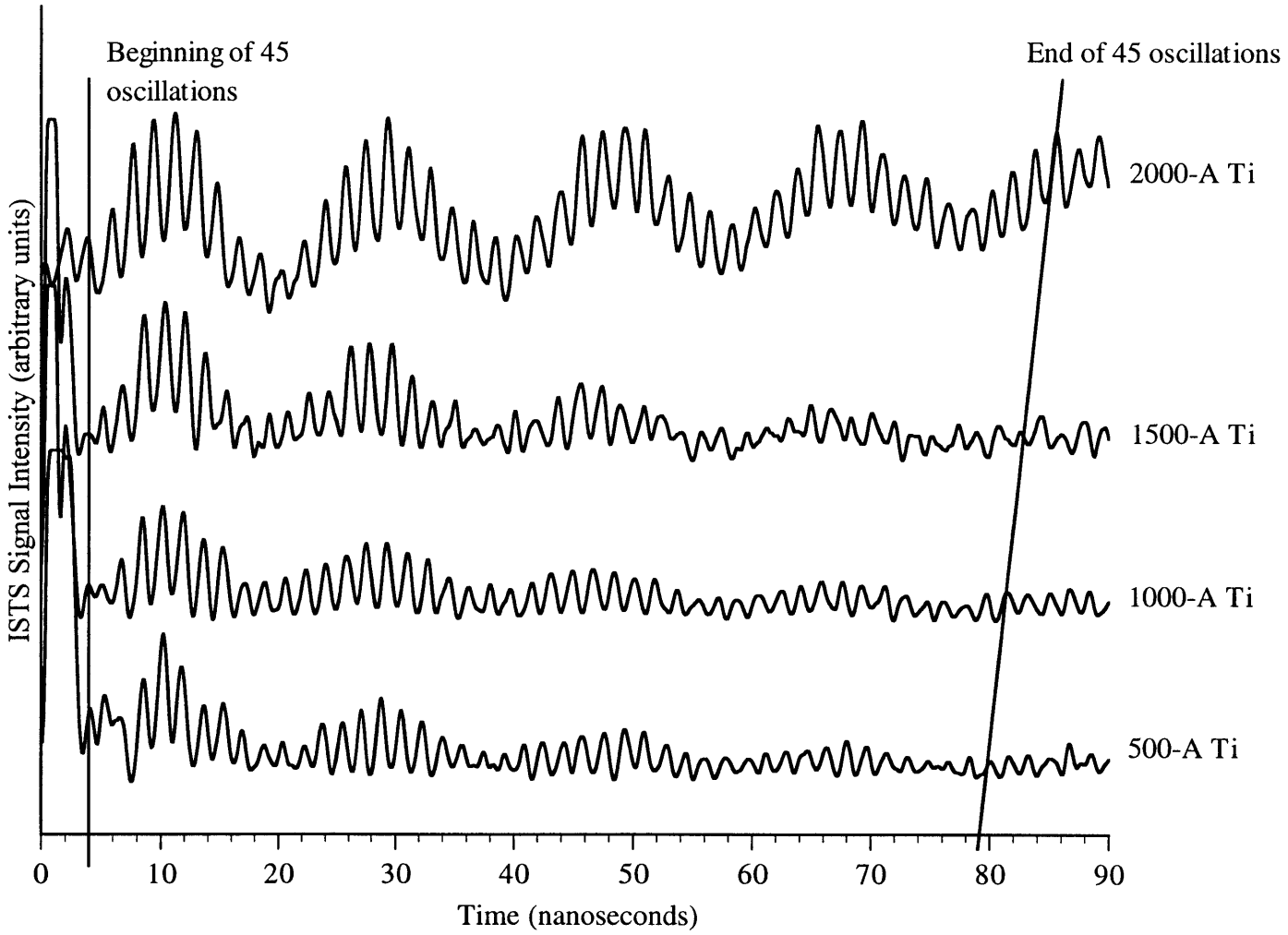

Figure 6: ISTS signal for varying thicknesses of titanium on silicon. Grating wavelength, Λ=8μm. Vertical lines represent the beginning and end of 45 oscillations and show a small increase in frequency with decreasing thickness.

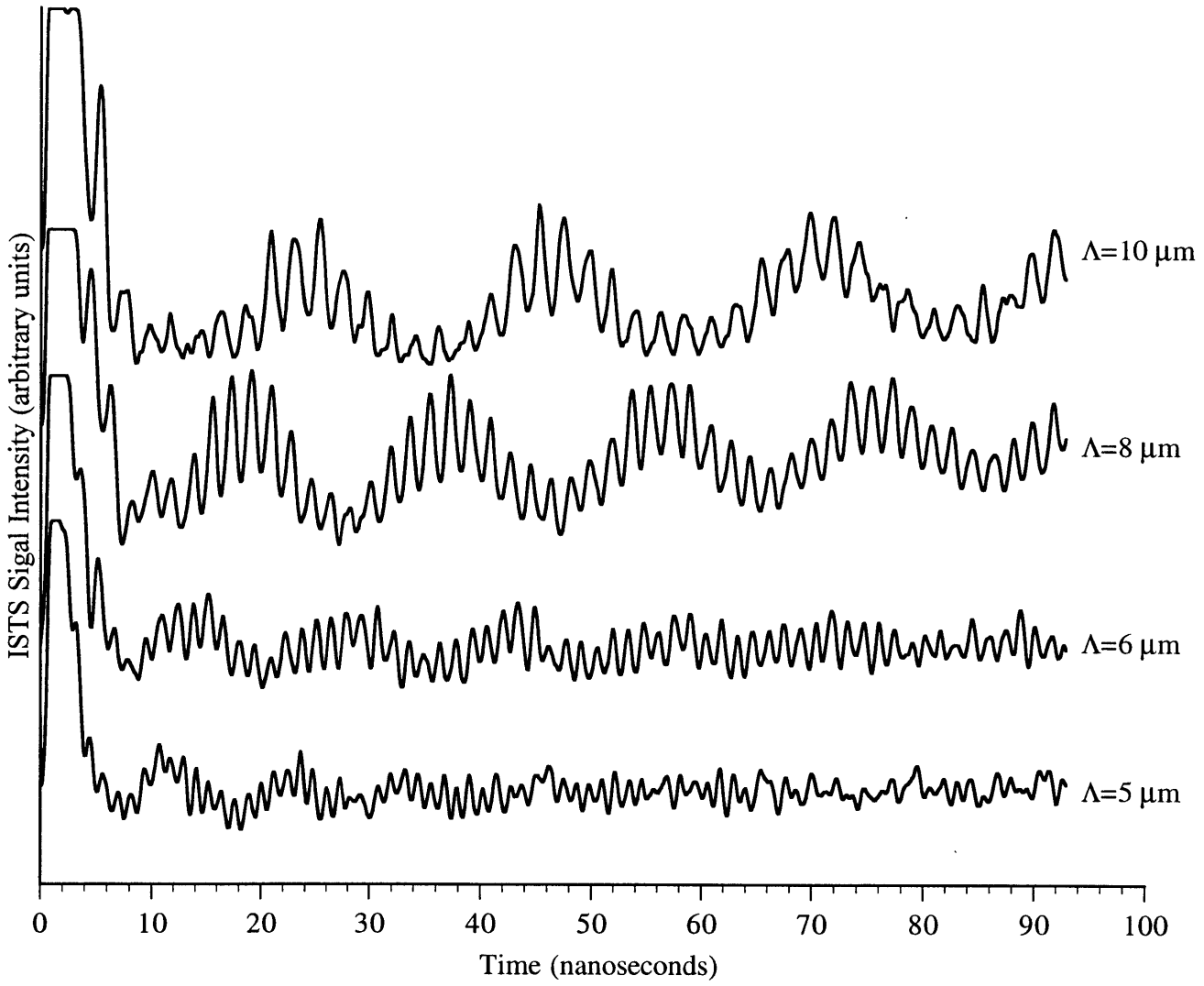

Figure 7: ISTS signal from 2000-A titanium on silicon for various acoustic wavelengths. Note the increase in frequency with a decrease in grating period wavelength, Λ.

the excitation pulse arrives and the sample has expanded, heat begins to flow from the heated regions to the unheated regions and the underlying films or substrate at a rate defined by the thermal diffusivity of the material. This "washing away" of the thermally expanded regions in seen in the data as the underlying exponential decay upon which the acoustic frequency modulates. Figure 8 shows a polyimide film which demonstrates the thermal decay rate very well. The data was taken at an excitation angle, θ_E, of 3.39° and an excitation wavelength, λ_E, of 355nm. The function drawn over the signal represents a single exponential decay, $A\exp^{-\Gamma t}$. If only thermal diffusion from peaks to nulls is considered, the decay of the signal should obey the relation, $I(t) \propto \exp(-2q^2 D_T t)$. From this expression, the thermal diffusivity, D_T, equals $\Gamma / 2q^2$. In the case of the polyimide in the figure, Γ=1.07 μs^{-1}, q=1.05 μm^{-1}, which gives a thermal diffusivity, D_T, equal to 0.49 $\mu m^2/\mu s$.

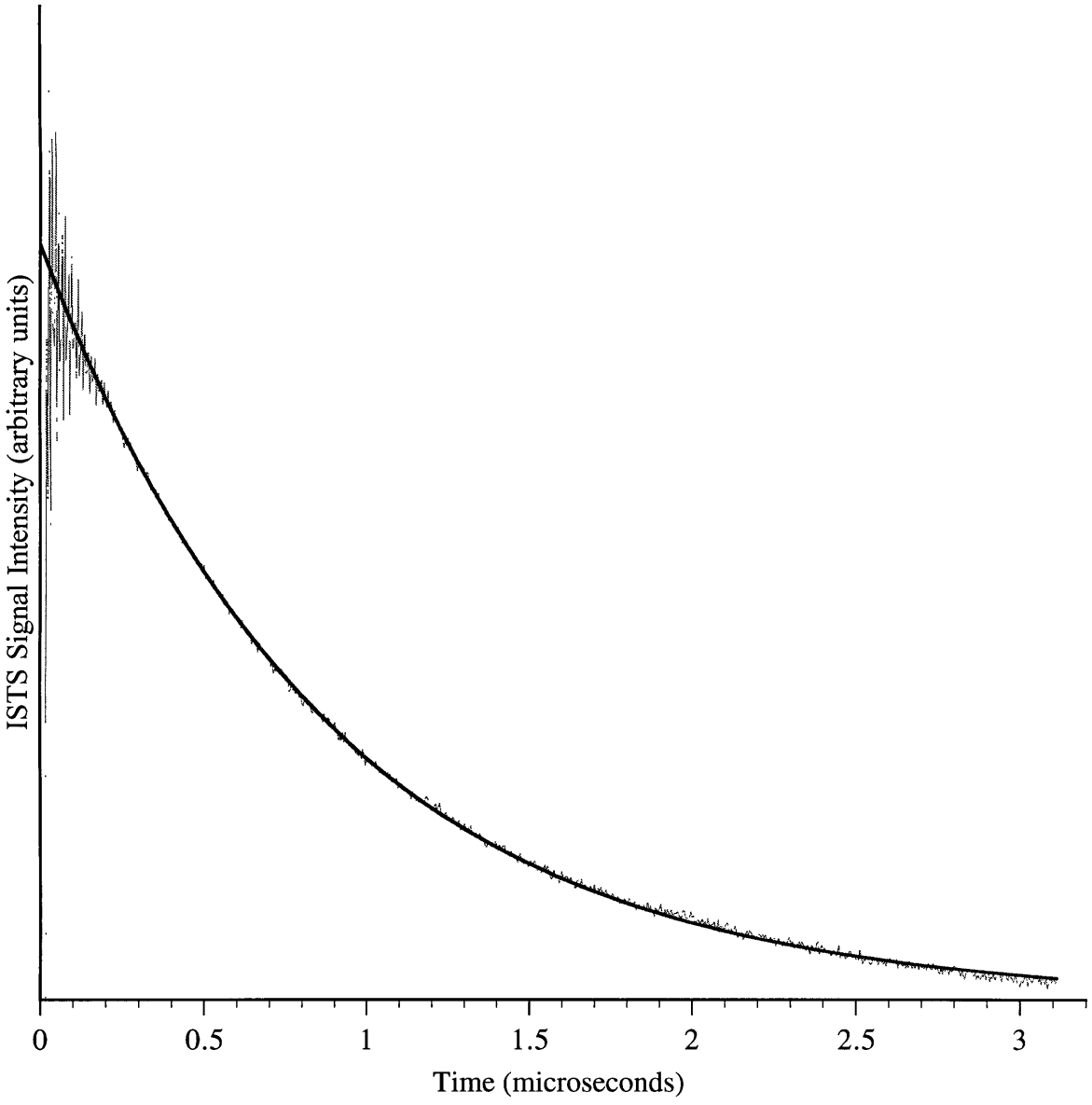

Figure 8: ISTS signal from Kapton polyimide. Acoustic oscillations are seen in the first 0.25 microseconds followed by thermal decay out to 3 microseconds. The solid line represents the thermal decay with the equation $A\exp(-\Gamma t)$.

Chapter 3: Metal Film Thickness Determination Using ISTS

3.1 Introduction

Process control over new generations of integrated circuits (IC's) becomes more challenging as larger wafers are processed to generate ICs with smaller feature sizes. In particular, thickness and uniformity of thin films are process-control parameters measured throughout the fabrication process [16]. Standard metrology instruments such as ellipsometers and reflectometers are commonly used to make non-contact thickness measurements of oxide layers, which are transparent to visible and infrared wavelengths [17,18]. However, non-contact measurement of the thickness of opaque metal films is a much more difficult problem. Metal films are used throughout IC fabrication as diffusion barriers and electrical contacts. Thickness variations can alter a film's mechanical and electrical properties, thereby affecting the performance of the circuit. Most monitoring of metal film uniformity is done by measuring monitor wafers with an electrical 4-point probe to determine electrical sheet resistance, which is proportional to the film's thickness [19]. X-ray-based techniques measure the thickness of metal films by inducing, measuring and analyzing X-ray fluorescence. X-ray fluorescence (XRF) measurements can determine absolute metal film thickness without contacting the sample, but are typically relegated to monitor wafers because of the slow speed (typically tens of seconds per point) and poor spatial resolution (usually greater than a few hundred microns) of conventional XRF instruments. In addition, XRF instruments are very large and expensive, generate hazardous X-rays and rely on an empirical measurement technique that requires extensive calibration.

Two other techniques that measure metal film thickness, scanning or transmission electron microscopy (SEM or TEM) and stylus profilometry, are commonly used in research-and-development environments. SEMs or TEMs accurately measure film thickness, but are

tedious to use and require destruction of the sample. Also, the procedure used to prepare a sample for SEM or TEM is typically cross-sectioning by cleaving or ion-milling. This destructive sectioning can alter the sample and affect the accuracy of the thickness measurement with this technique [20]. Profilometry measures relative changes in surface height by dragging a stylus across a small area on the sample's surface. While accurate and having high spatial resolution, this technique is slow, requires contacting the sample, cannot measure absolute film thickness, and is sensitive to wafer curvature.

In summary, the microelectronics industry currently lacks a metrology instrument that can rapidly make high-resolution *in situ* or *ex situ* measurements of metal film thickness on actual product wafers. Such measurements are desirable for several reasons. First, monitor wafers are not salable product, are very expensive to process, and supplant processing time and resources that would otherwise be used for actual product wafers. Second, as manufacturing processes use larger wafers to make devices with smaller feature sizes, monitor wafers become less representative of the real problems associated with product wafers [16]. Thus, when a monitor wafer falls outside of a manufacturer's specifications, the product wafers associated with that monitor wafer are tracked down and labeled as suspect. The subsequent testing process is often difficult and costly in terms of reduced yield and lost value added. Clearly, performing process-control measurements on metal films deposited directly on product wafers will save manufacturers both time and money.

Over the last several years, a novel, all-optical method for measuring mechanical, physical, and thermal properties of thin films has been developed. Initial research for this project began at MIT with the goal of characterizing the elastic and thermal transport properties of polymer films; more recently this method has been incorporated in a commercial instrument for determining the thickness and uniformity of opaque metal films used in ICs. The instrument measures a range of properties which, until now, could only be accessed with multiple

instruments. For example, the instrument measures film uniformity like a 4-point probe, thickness of small-scale features like a stylus profilometer, and absolute film thickness like an X-ray fluorescence instrument. Unlike these competing tools, measurements are made with all the advantages normally associated with optical instrumentation: non-contact measurements are made rapidly (less than one second per point), with high spatial resolution (less than 50 microns), and can be made remotely (i.e. from outside of a vacuum chamber). The instrument can therefore test actual product wafers, rather than only monitor wafers, thereby increasing the throughput of actual salable product. Metal films ranging from adhesion-promoting metallization layers (i.e. ti:nitride) to electrical contacts (i.e. aluminum) can be measured with the instrument.

In this work, we demonstrate determination of metal film thickness using a method that is fast, non-contact and non-destructive. Measurements have been performed on a number of materials and structures in order to assess the sensitivity and versatility of the technique. Comparisons to the results of other measurement methods have been made to validate the technique.

3.2 Experimental Setup - Compact Apparatus

A compact ISTS experimental setup is shown schematically in figure 9. A 1.2-W diode laser pumps a passively Q-switched, single-mode Nd:YAG microchip laser [21,22], yielding 1064-nm excitation pulses of 400-picoseconds duration with 10 μJ of energy and a repetition rate of 125 Hz. This repetition rate is chosen to be high enough for fast data averaging (to maximize signal to noise) and low enough to allow the film's temperature to return to ambient between excitation laser shots. Because acoustic waves will be excited in any material that absorbs the excitation radiation, the ISTS measurement can be used on nearly all metals and semiconductor films. The pulses are cylindrically focused to a spot size of 50 μm x 250 μm onto a phase mask pattern consisting of evenly spaced grooves etched to a depth of $\lambda/4$ into a glass substrate.

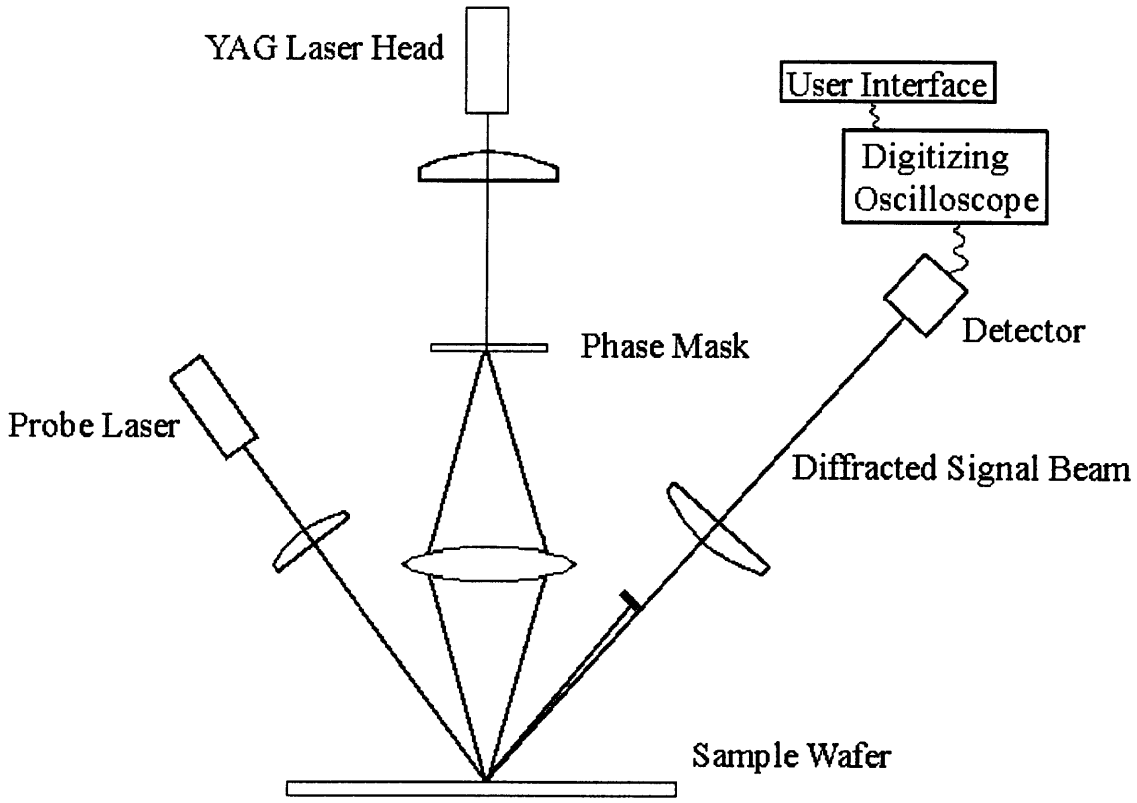

Figure 9: Optical schematic for compact ISTS experimental setup.

Diffraction off the pattern directs over 80% of the laser energy into the ±1 orders. The diffracted pulses are collected with a 1:1 imaging lens and recombined at the surface of the sample where they produce the grating interference pattern. Many mask patterns are available on a single glass substrate so that the interference fringe spacing and the acoustic wavevector can be varied simply by moving the desired pattern into the excitation beam path. In past experiments, a beam splitter was used to create two beams. These two beams would then be reconverged at the sample's surface after traveling an identical distance to ensure temporal overlapping of the pulses. The phase mask design has many advantages over conventional optics. In particular, the phase mask reduces the number of optical components (i.e. lenses, mirrors, beam splitters) required which, in turn, reduces the necessary size of the optical system. Also, the phase mask reduces the number of moving parts in the optical system by requiring only a one-dimensional translation to achieve different angles. In contrast, the conventional optical system requires many moving parts to ensure that the lengths of the beam paths traveled by the two pulses are identical. An optical system containing fewer moving parts is desired in order to maximize automation capabilities and minimize user intervention in the final instrument.

The probe consists of an 860-nm diode laser, modulated to yield a quasi-cw probe pulse which is timed to begin before the excitation pulses reach the sample and end several microseconds after the material returns to its undisturbed state. The probe beam is focused to a spot size that is smaller than that of the excitation spot size in order to maximize the level of signal collected. The probe beam is diffracted off the spatially and temporally varying surface ripple and the diffracted signal is detected in reflection mode and temporally analyzed using a high-bandwidth amplified photodiode and digitizing oscilloscope.

The entire optical apparatus including the lasers fits onto a 1 ft x 2 ft breadboard, and requires only wallplug electrical power and no cooling water. The small footprint of the optical apparatus is desirable in a potentially in-line instrument because space is extremely valuable in

most film forming and processing instrumentation. For example, the metrology instrument could potentially be attached directly to a film-formation tool (chemical vapor deposition, plasma-vapor deposition) or a film processing tool (chemical-mechanical polisher). The optical beams could pass through optical ports on the film tools, allowing measurements to be made while the film is under vacuum and being transported using a wafer handling system that is already present.

3.3 Typical Samples and Measurement Requirements

Market research and communication with potential customers of ISTS technology has produced a set of guidelines which defines the material types and measurement precision and accuracy desired. Table 1 shows the typical metals used in integrated circuits, their function, thickness range and the required precision for a thickness instrument. The 0.2% precision comes from the fact that tools used to make these layers have an uncertainty of approximately 1%. In order for a metrology instrument to be of any value in measuring a film with a 1% uncertainty, it must be capable, in the best case, of measuring with a 0.2% uncertainty for these films.

Material	Function	Thickness Range (A)	Precision Needed (0.2%) (A)
Aluminum	Interconnect	4,000-20,000	8-40
Tungsten	Plug, vertical wiring	4,000-12,000	8-24
Titanium:Tungsten	Plug, vertical wiring	250-750	0.5-1.5
Titanium	Contact, adhesion promoter	200-1500	0.4-3.0
Titanium:Nitride	Adhesion promoter, AR coating, barrier	200-750	0.4-1.5
Tungsten:Silicide		4,000-8,000	8-16
Copper	Interconnect	4,000-20,000	8-40

Table 1: Materials used in microelectronic circuits with typical thickness ranges and desired thickness measurement precision [23].

3. 4 Comparison To Other Thickness Measurement Techniques

3.4.1 Profilometry

In order to simultaneously demonstrate the sensitivity of ISTS to thickness changes and the spatial resolution of the technique, a titanium test structure was fabricated. The test structure is a 1200-A electron-beam evaporated titanium layer on silicon with titanium steps of various heights in a grating pattern deposited on top. Figure 10a is a 3-D plot derived from ISTS measurements of this structure. The steps in the figure are 640 A in height and the spacing between the steps is 250 μm. The z-axis of the plot gives the thickness of the titanium layer at various points on the structure, determined from ISTS measurements of acoustic frequency and the bulk Ti elastic and density values and minor (1-2%) calibration of the grating wavevector based on the nominal 1200-A thickness. Figure 10b is a 2-D plot of stylus profilometry results measured along a line which cut across the titanium steps. The correlation between profilometry and ISTS results is apparent. Note that profilometry only measures relative changes in surface height while ISTS has the ability to determine both relative changes in surface height and absolute thickness provided the elastic properties of the different layers are known. Figure 11 shows the same measurements on a structure whose steps are 320-A in height. Though not as distinct as in the previous figure, the steps are clearly resolvable and demonstrate the ability of the technique. Figure 12 again compares the ISTS measurement to stylus profilometry but on a structure whose step height is 150 A. The data also demonstrate the spatial resolution of ISTS, determined in this case by the spot size of 50 μm x 200 μm at the sample.

3.4.2 Scanning Electron Microscopy (SEM)

ISTS measurements also were conducted on several films of an Al(1% Cu) alloy sputtered onto silicon wafers. The wafers were then fractured and cross sections were examined

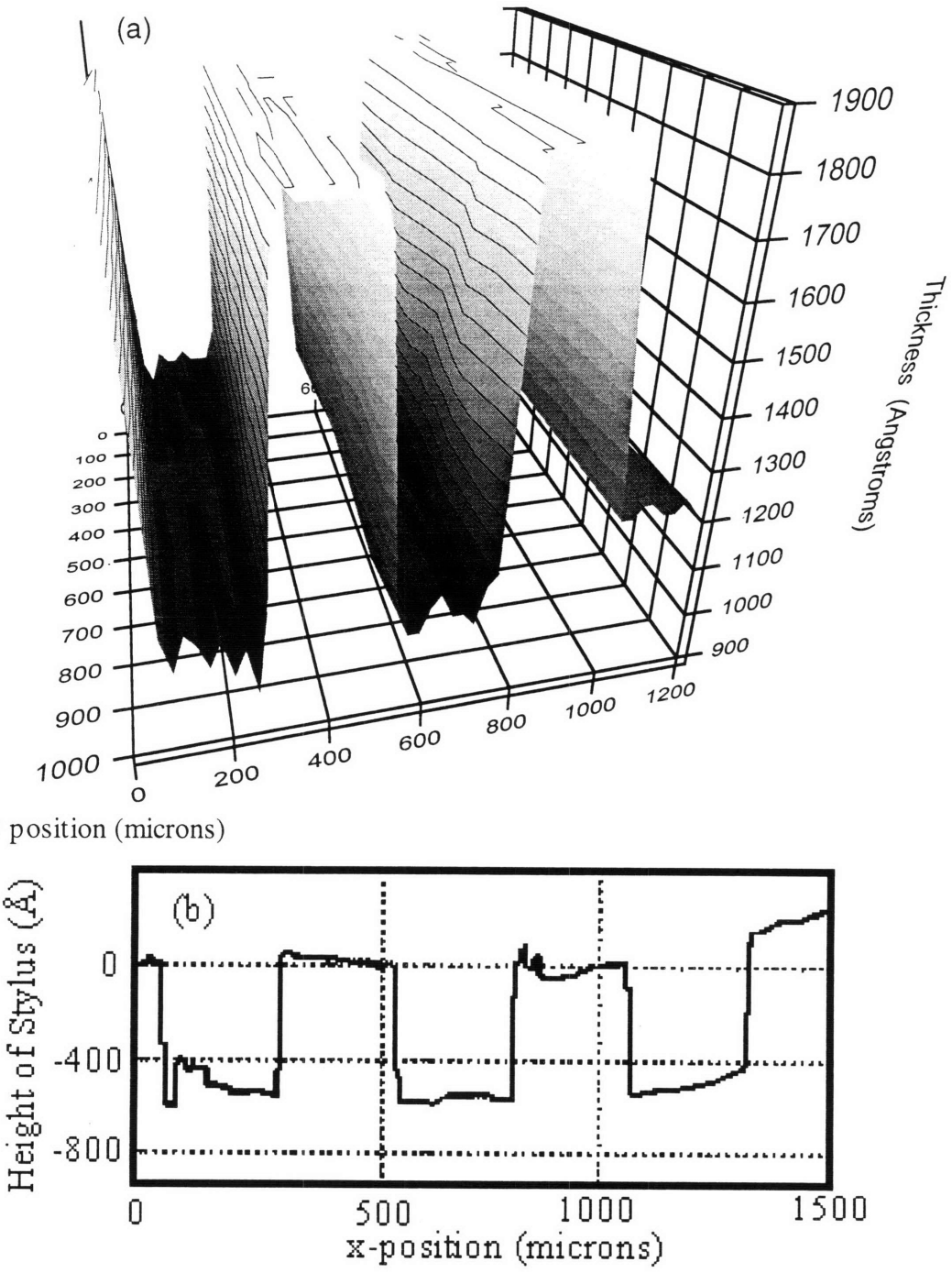

Figure 10: (a) ISTS data on 1200-A titanium with 640-A titanium steps deposited on top. (b) Profilometry trace of same structure. Note how profilometry only measures relative surface heightt while ISTS measures absolute thickness.

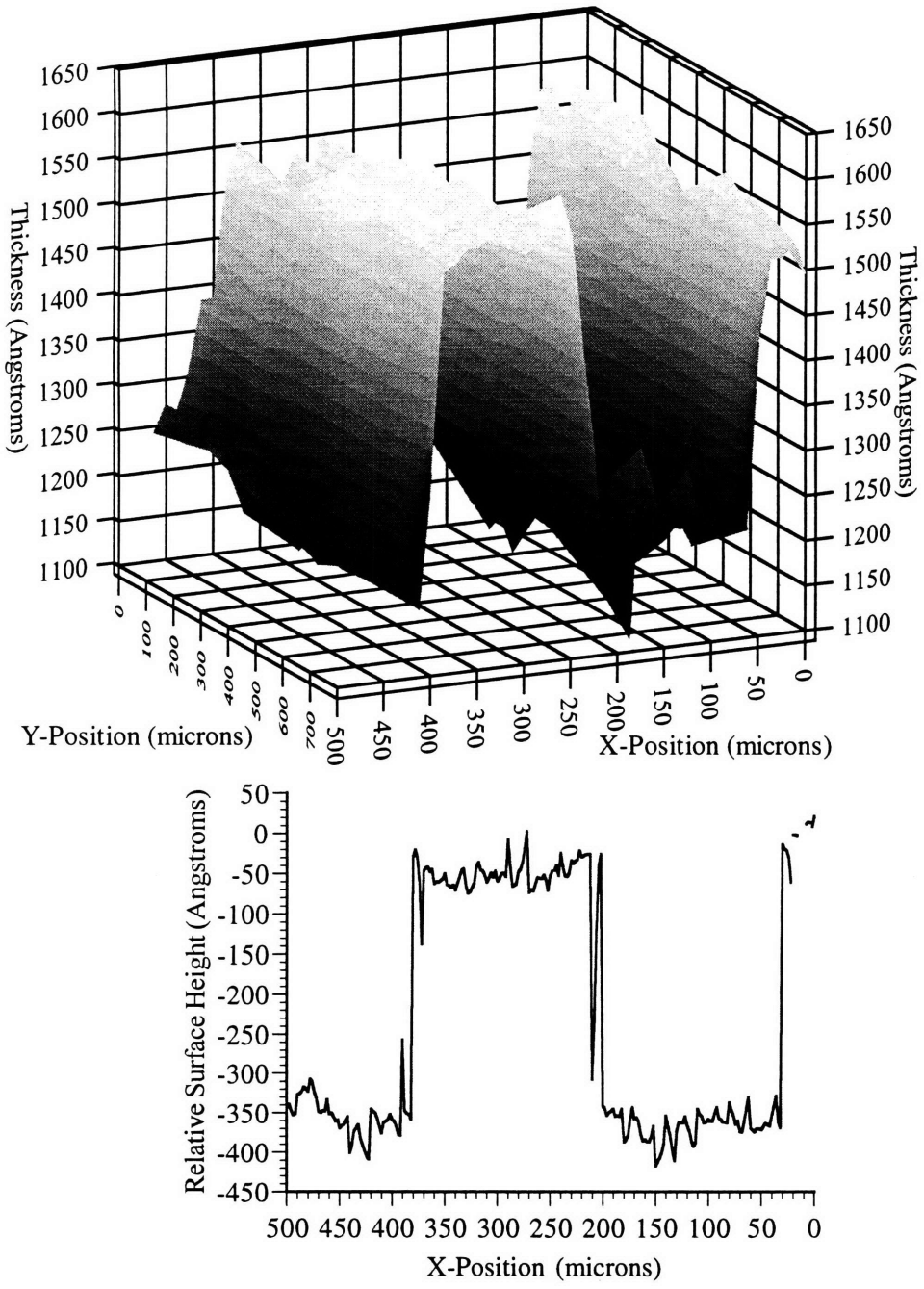

Figure 11: (a) ISTS data on 1200-A titanium with 350-A titanium steps. (b) Profilometry data on same structure. Note how ISTS measures total thickness while profilometer onle measures relative surface height.

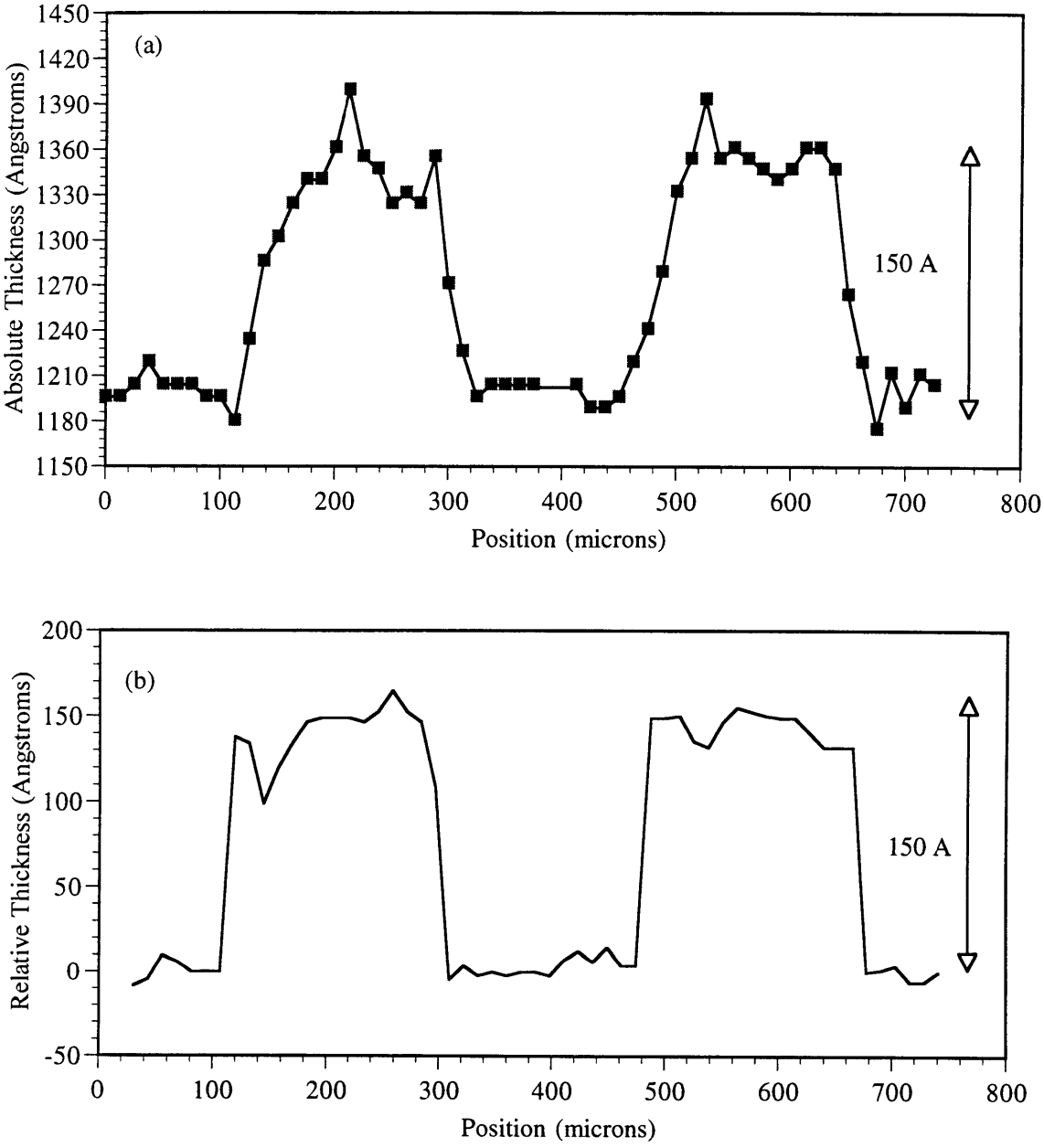

Figure 12: (a) ISTS versus (b) stylus profilometry on a 1200-A titanium film with 150-A steps deposited on top.

with a scanning electron microscope to determine the AlCu film thicknesses. Figures 13-15 show three electron micrographs with the corresponding thickness measured on the micrograph. Table 2 presents the SEM results along with the film thicknesses calculated from ISTS data taken at points close to where the SEM cross sections were analyzed. All three AlCu films were assumed to have the same values of density and elastic moduli, slightly different from the bulk Al values for these calculations. The differences seen between SEM and ISTS here are easily accounted for by several sources of error. First, measurements were not necessarily made at the exact same point on the wafer. A positional error of a few hundred microns between where the SEM and ISTS measurements were made is entirely possible. Variations in the ISTS data in the region where the SEM measurements were made were enough to cause such differences in thickness calculations. Also, the mechanical properties (sound velocities and density) could change with thickness enough to cause substantial errors in the thickness calculated by the thermoelastic equations of motion. Film thickness measurements made with SEM (and TEM) are typically considered the most reliable method for film thickness determination but the method used to prepare samples, either cleaving or ion-milling, can affect the accuracy of the thickness measurement [20].

	Film 1	Film 2	Film 3
SEM Thickness	1240-A	4200-A	8100-A
ISTS Thickness	1400-A	4200-A	8200-A

Table 2: SEM thickness and ISTS thickness of AlCu films on silicon.

3.4.3 4-pt. Probe

4-point electrical resistivity measurements are commonly used to measure metal film thickness in microelectronics. In the measurement, current and voltage are measured between probes spaced very closely to determine sheet resistance which is proportional to thickness [19]. ISTS 49-point scans were performed on tungsten wafers in order to investigate the correlation between 4-point probe and ISTS measurements. Figure 16a shows a wafer map generated using

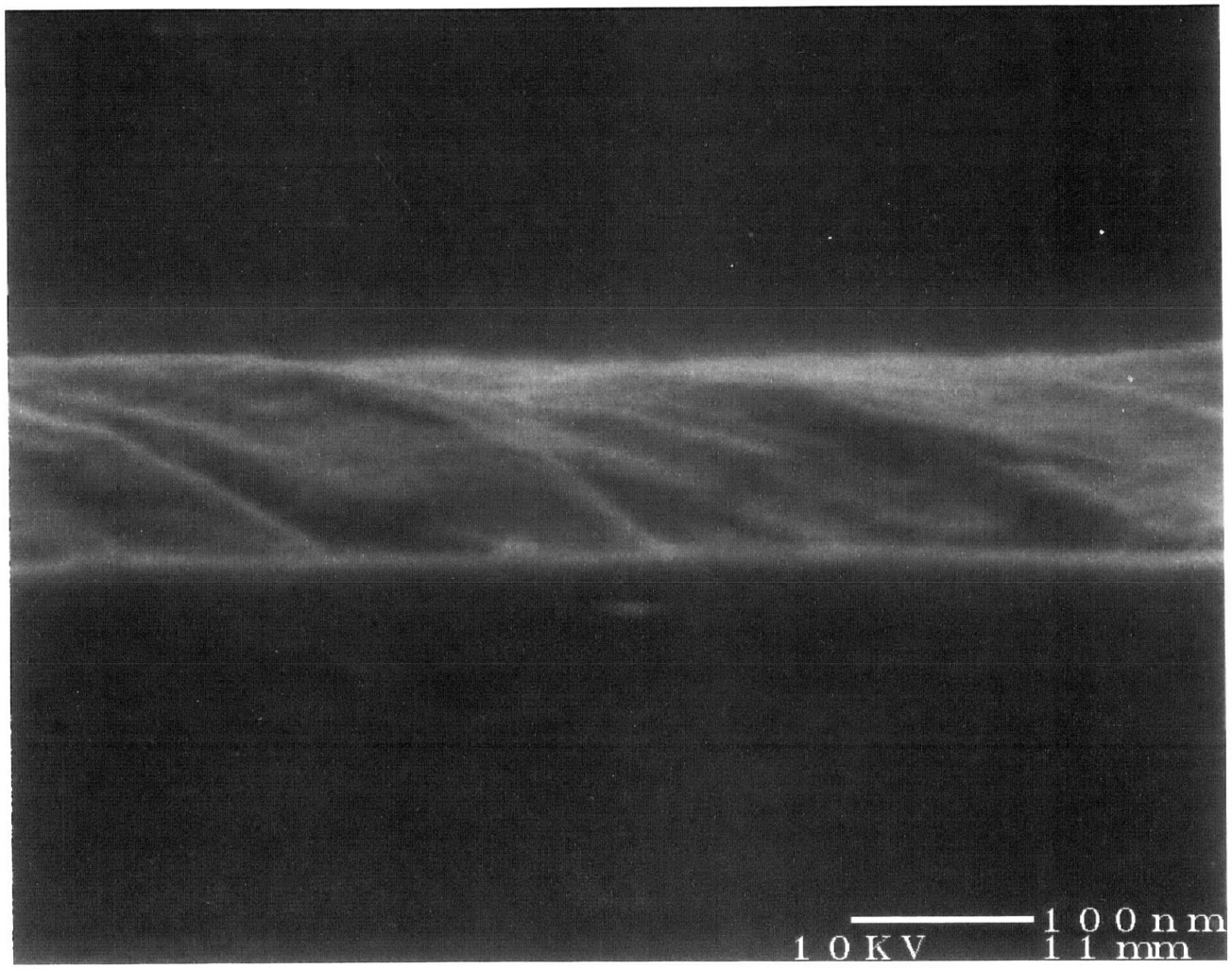

Figure 13: SEM micrograph of Al(1%Cu) on silicon. Thickness measured at 1240 A.

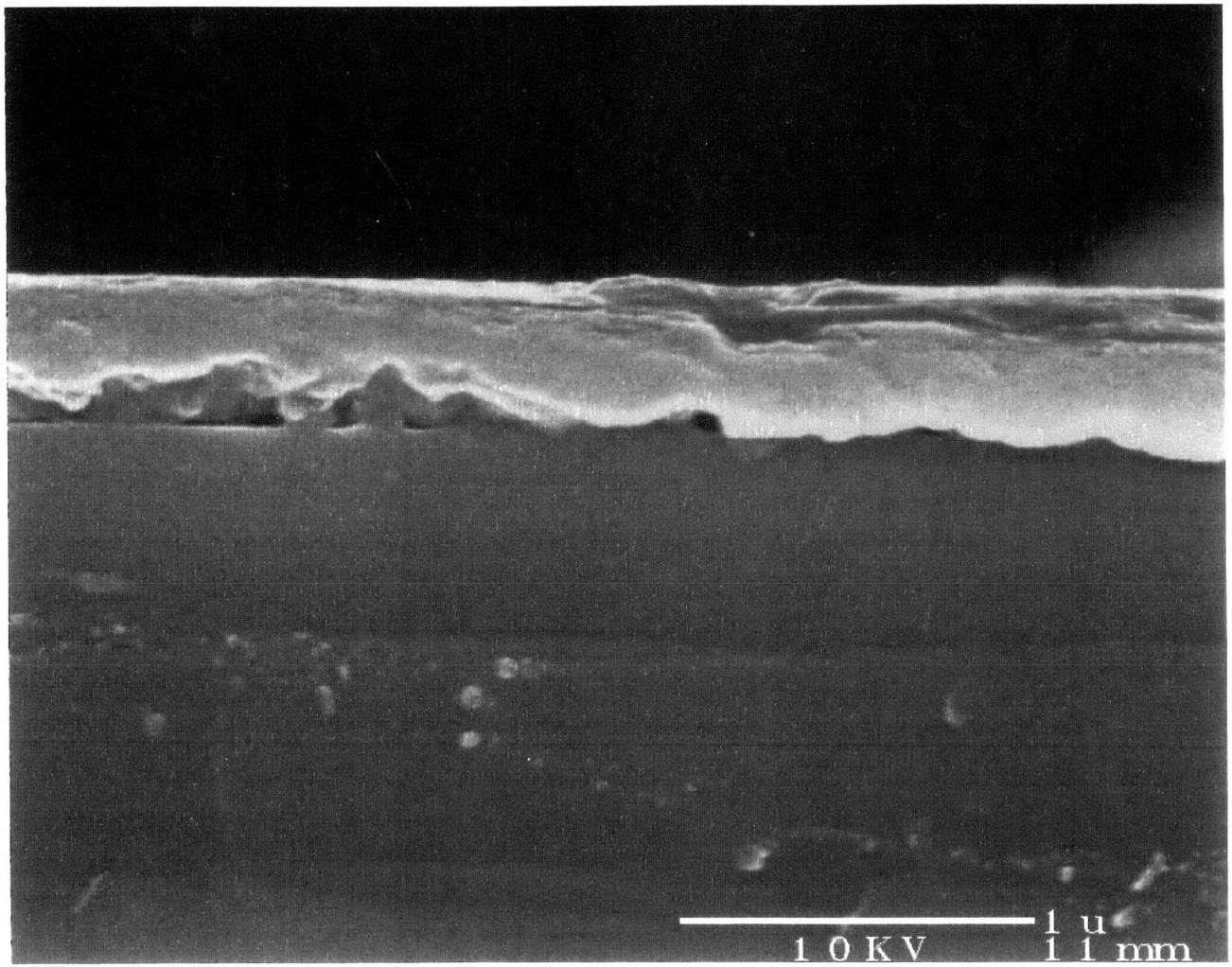

Figure 14: SEM micrograph of Al(1%Cu) on silicon. Thickness measured at 4200 A.

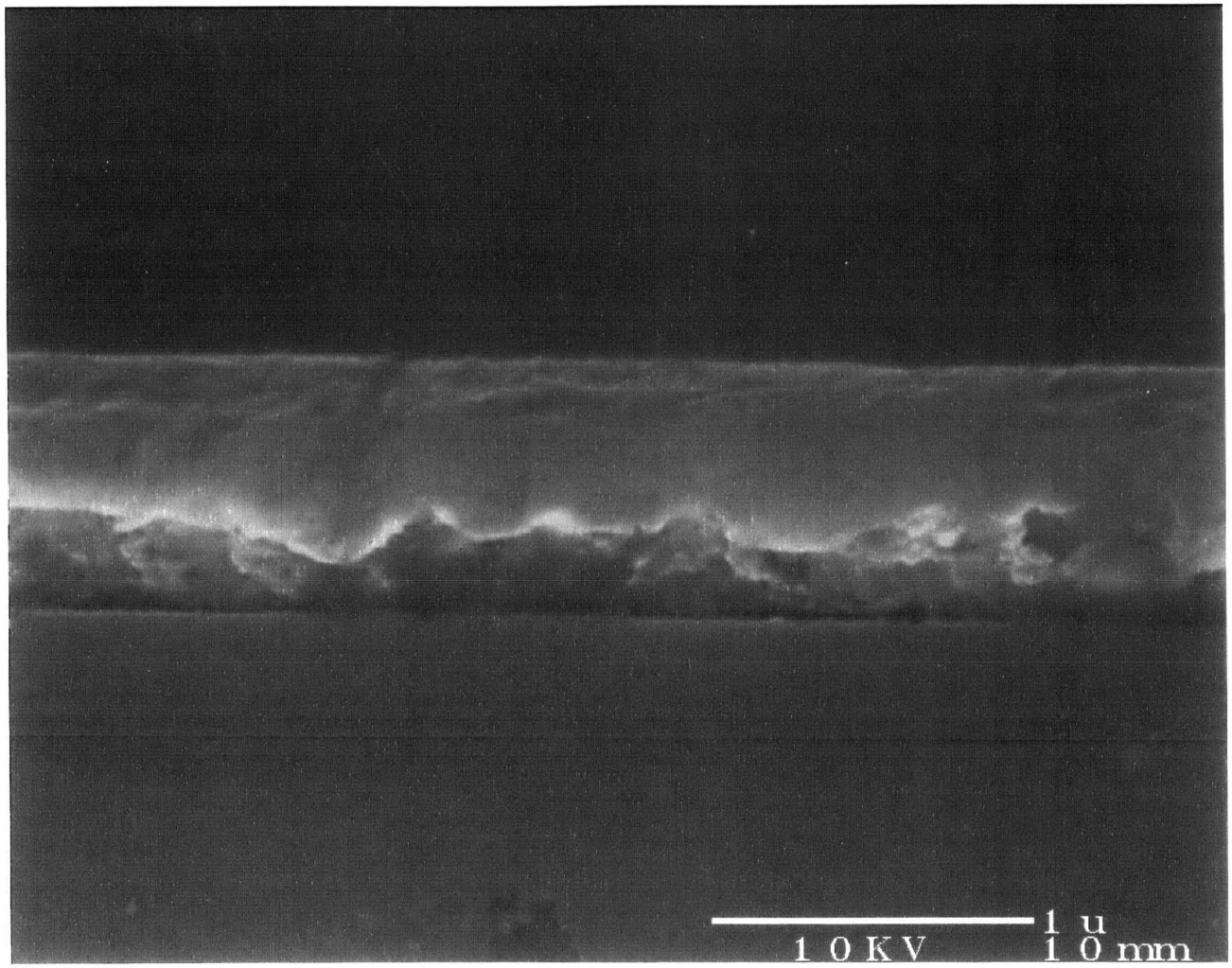

Figure 15: SEM micrograph of Al(1%Cu) on silicon. Thickness measured at 8100 A.

ISTS with thickness contours for a tungsten film of 5000-A nominal thickness deposited on silicon. The contour maps shown were generated using a numerical smoothing routine which averaged over five measurements on nearby points to calculate the results shown. This eliminated point irregularities which may have been due to dust particles (which mechanically "load" the local region of the film, and thereby alter the measured acoustic frequency) on some wafer positions. Such averaging may be less important in a cleanroom environment. The W:Si assembly also was analyzed with a 4-point resistance probe whose results are shown in figure 16b. The 4-point probe also uses a smoothing routine. The two scans are almost identical. Figure 17 shows the same comparison for a nominal 10,000-A tungsten film on silicon.

4-point probe measurements were also conducted on multilayer samples (titanium:tungsten on oxide on silicon and platinum on oxide on silicon). Comparisons between 4-point probe and ISTS on these samples are shown in figures 18 and 19. The comparisons made are between the raw values of each measurement technique instead of the thickness. This is done because the details of the structures are not fully understood and therefore conversion of the raw measurements to thickness values is not straightforward. The figure demonstrates that the measurement trends are similar on these samples and because of the correlations established earlier, it can be deduced that they are measuring the same parameter, which is film thickness. Figure 20 shows an attempt to correlate the thickness values of the two techniques on the first of these two samples based on an estimate of the structure to be 750-A of titanium-tungsten on 1000-A oxide on silicon. The correlation between the contours is preserved but the range of thickness values that result from conversion of the raw data is not the same. This result is probably due to the inherent difference in how the two techniques function. The 4-point probe measure measures only the Ti:W resistivity while ISTS probes the entire structure.

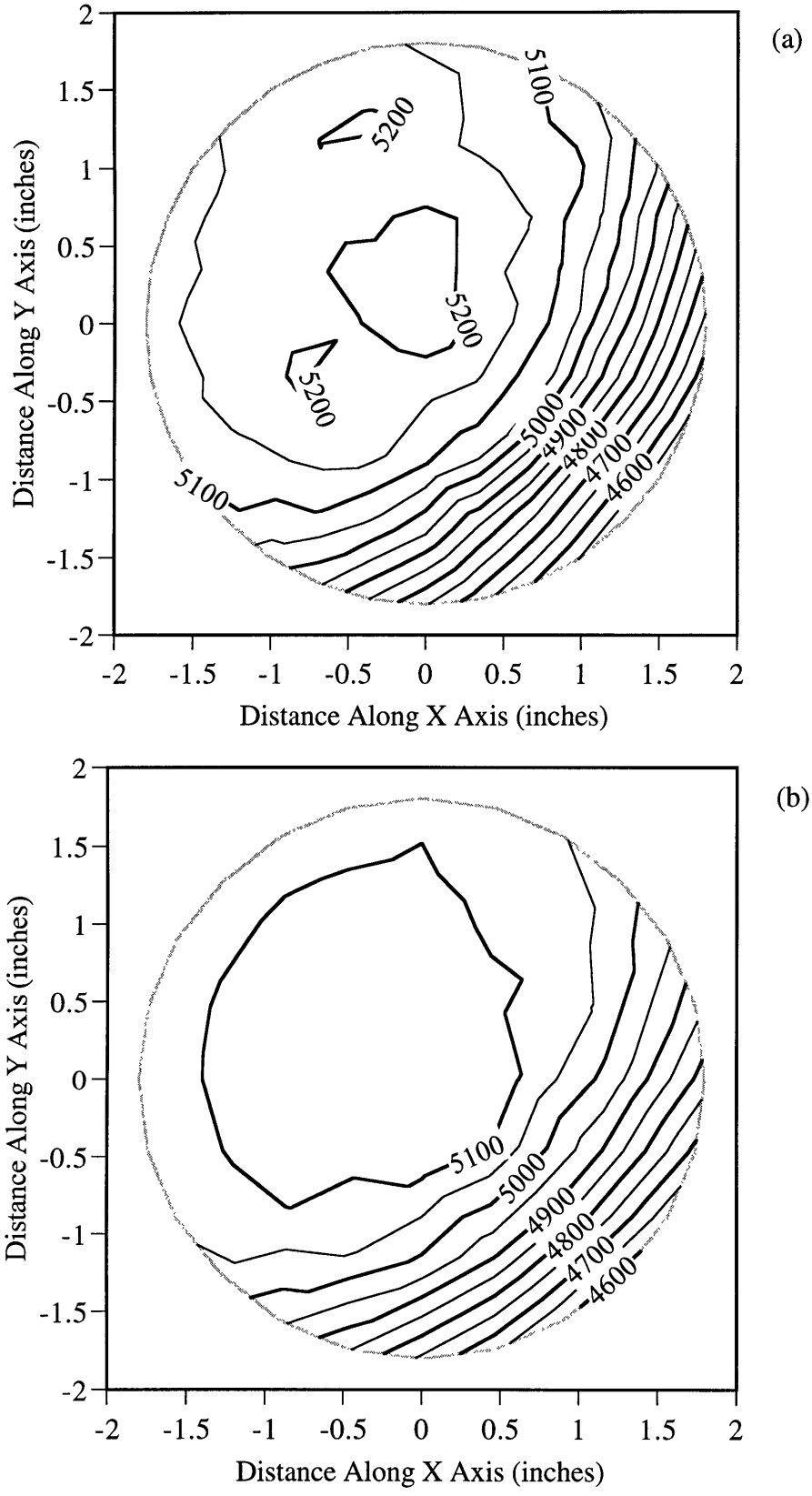

Figure 16: (a) ISTS versus (b) 4-point probe on a 5000-A tungsten film on silicon.

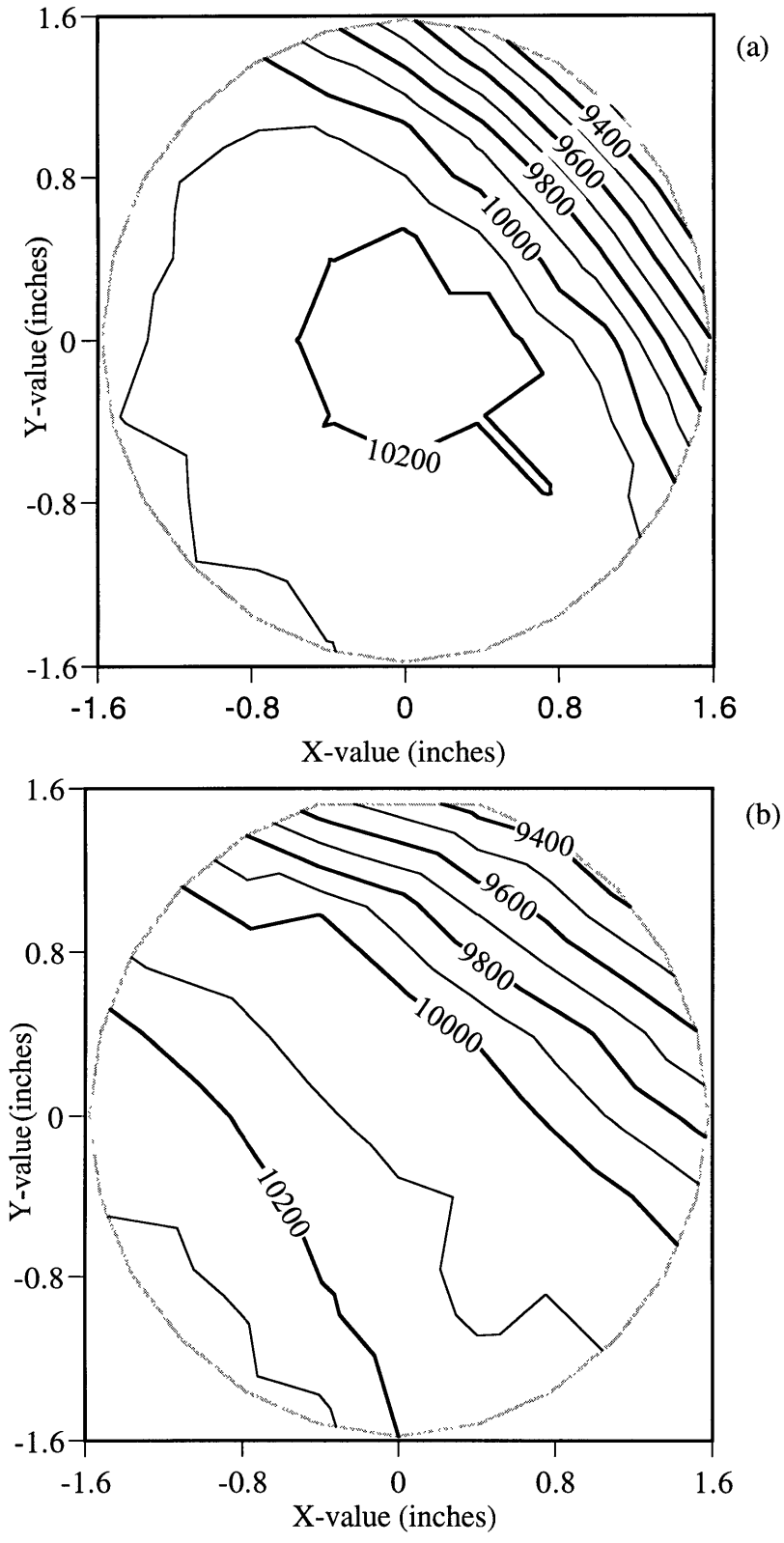

Figure 17: (a) ISTS versus (b) 4-point probe on a 10,000-A tungsten film on silicon.

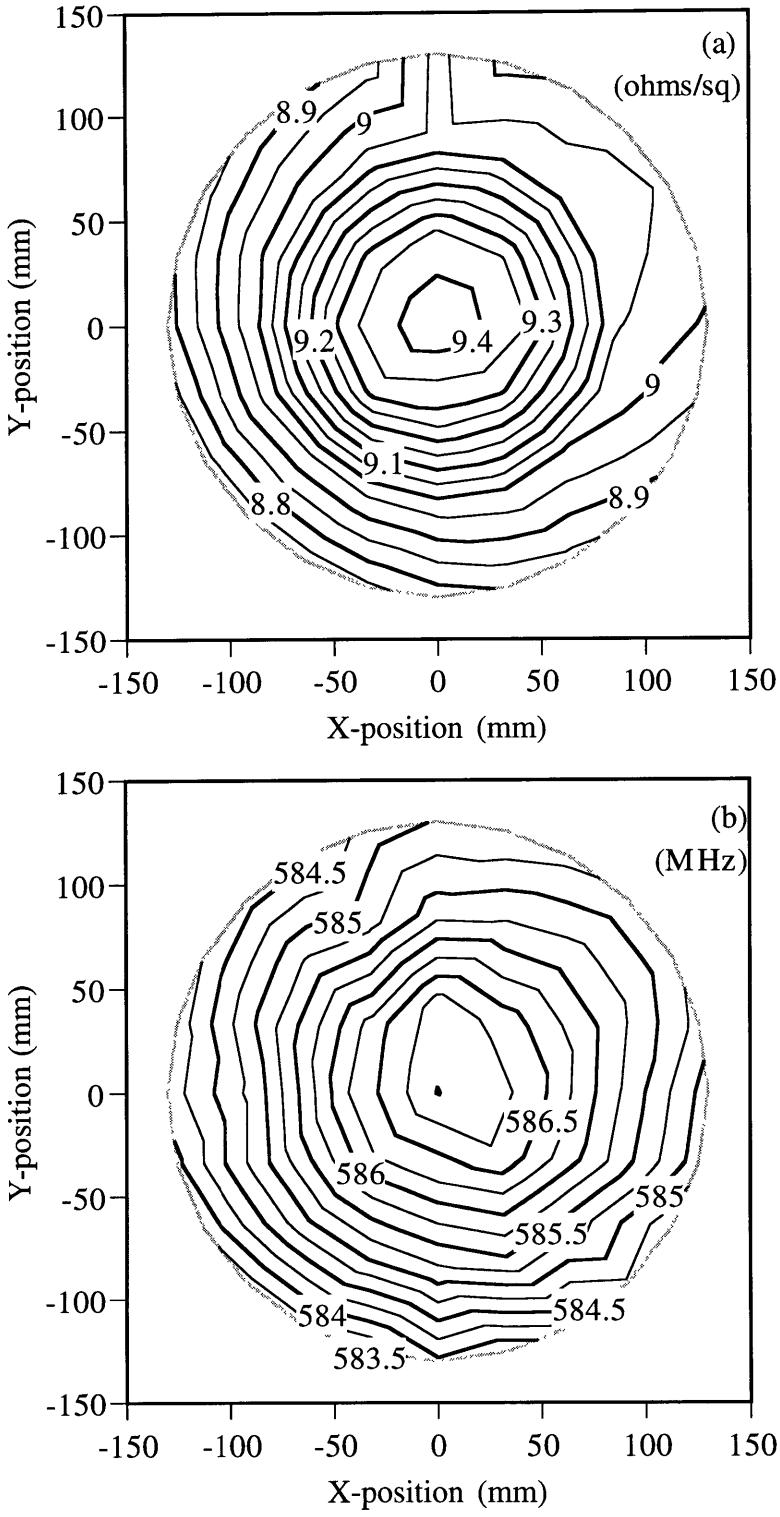

Figure 18: Contour maps of 750-A Ti:W on 1000-A oxide on silicon as deterined by (a) 4-point probe and (b) ISTS.

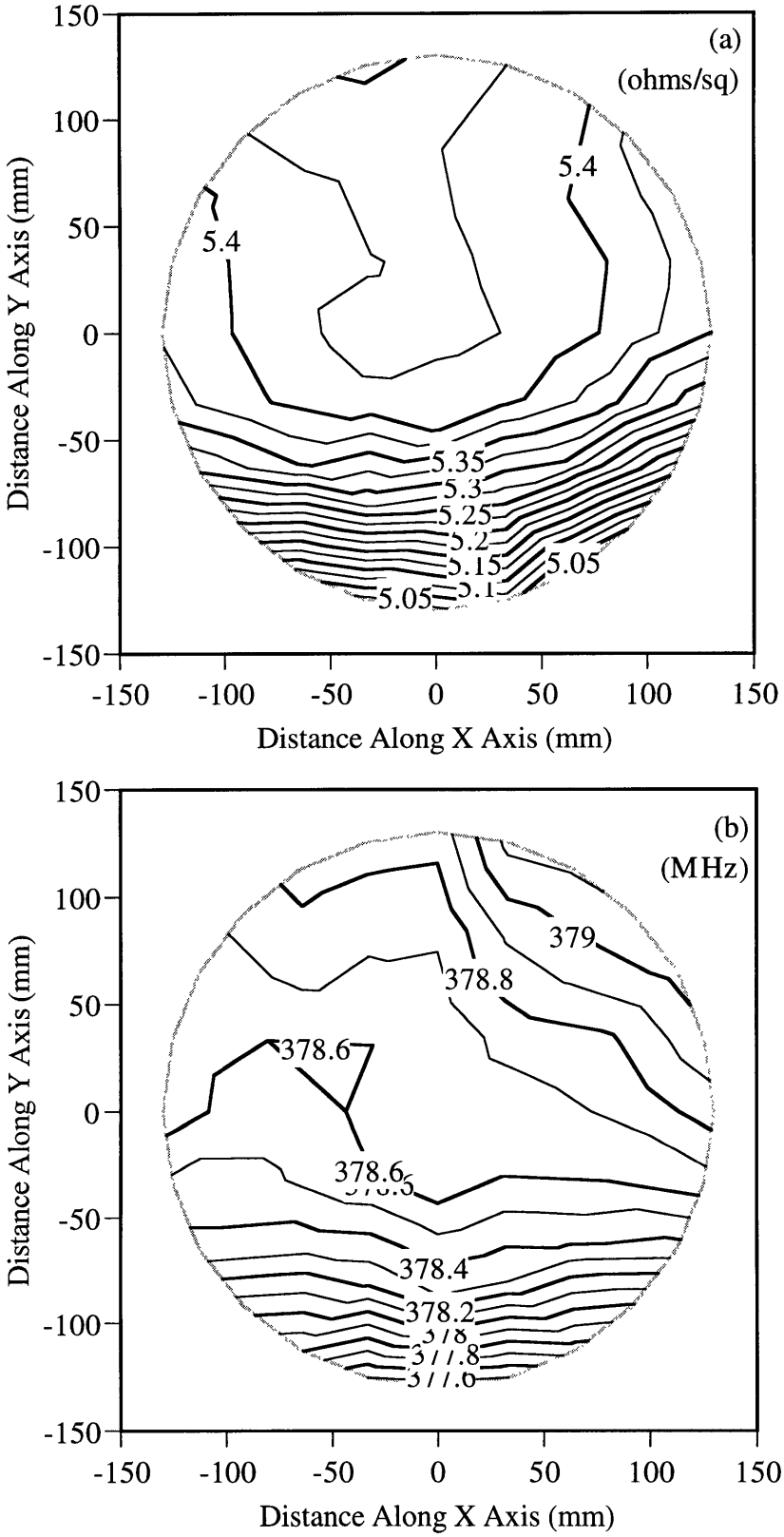

Figure 19: Contour maps of 400-A Pt on 2000-A oxide on silicon as determined by (a) 4-point probe and (b) ISTS.

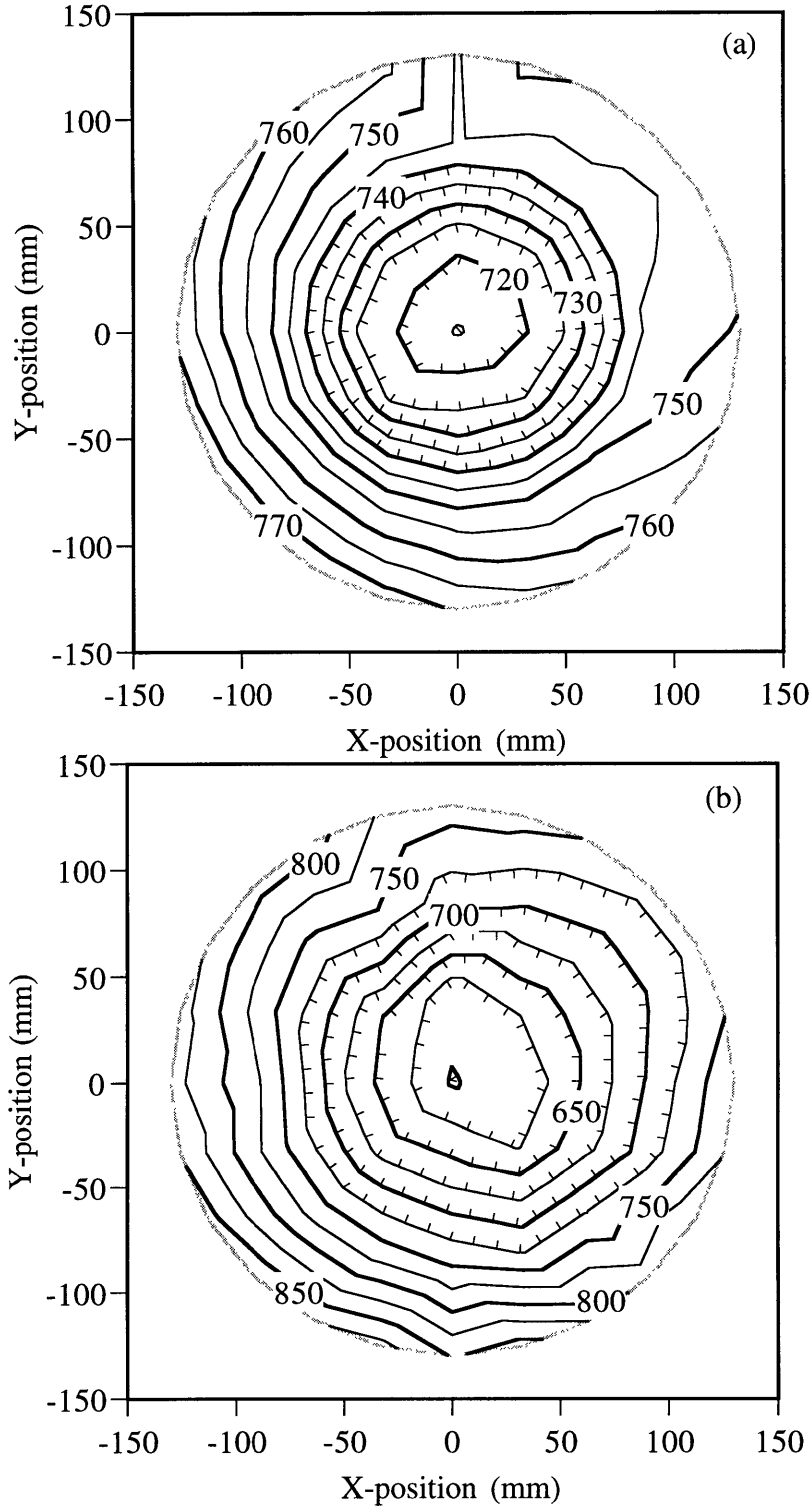

Figure 20: Thickness contour maps as determined by (a) 4-point probe and (b) ISTS on 750-A Ti:W on 1000-A oxide on silicon.

3.4.4 X-Ray Fluorescence

X-Ray fluorescence (XRF) is a technique commonly used to measure the thicknesses of thin films but has many disadvantages that were discussed earlier. In order to further benchmark the ISTS technique against instrumentation already accepted in the microelectronics industry, a titanium sample (nominal 1800-A titanium on 5000-A oxide on silicon) was sent to IBM analytical laboratories to be analyzed with XRF. The sample was then analyzed with ISTS at approximately the same points in order to establish a correlation. The ISTS measurements were calibrated by adjusting the wavevector, q, in order to get the thickness numbers to correspond to approximately the same range. Figure 21 shows the XRF measurements versus ISTS. Correlation between XRF and ISTS is good ($\pm$ 0.5%), however, a perfect correlation probably does not exist for several reasons. First, XRF is only sensitive in this case to the thickness of the titanium layer while ISTS is sensitive to the entire structure (oxide and substrate). Changes in oxide thickness or oxide or substrate mechanical properties across the wafer could theoretically affect the ISTS measurement although these variations are typically not substantial (see section 3.9). Second, XRF has very poor spatial resolution compared to ISTS. In comparison to ISTS, XRF measurements are essentially averages of thicknesses over large regions. The points measured with ISTS may have been in a region where the local thickness was different from the averaged thickness. Also, the ISTS result typically has more point to point variation, possibly a result of the small spot size of the measurement coupled with small scale local variations in optical properties, grain size, etc.

3.5 ISTS Measurement For Systematically Varying Samples

In order to qualify the ISTS measurement as a film thickness metrology technique, many sample sets were fabricated which contained systematically varying thicknesses of metal films in single- and multi-layer structures. Experiments were carried out to demonstrate the ability of the

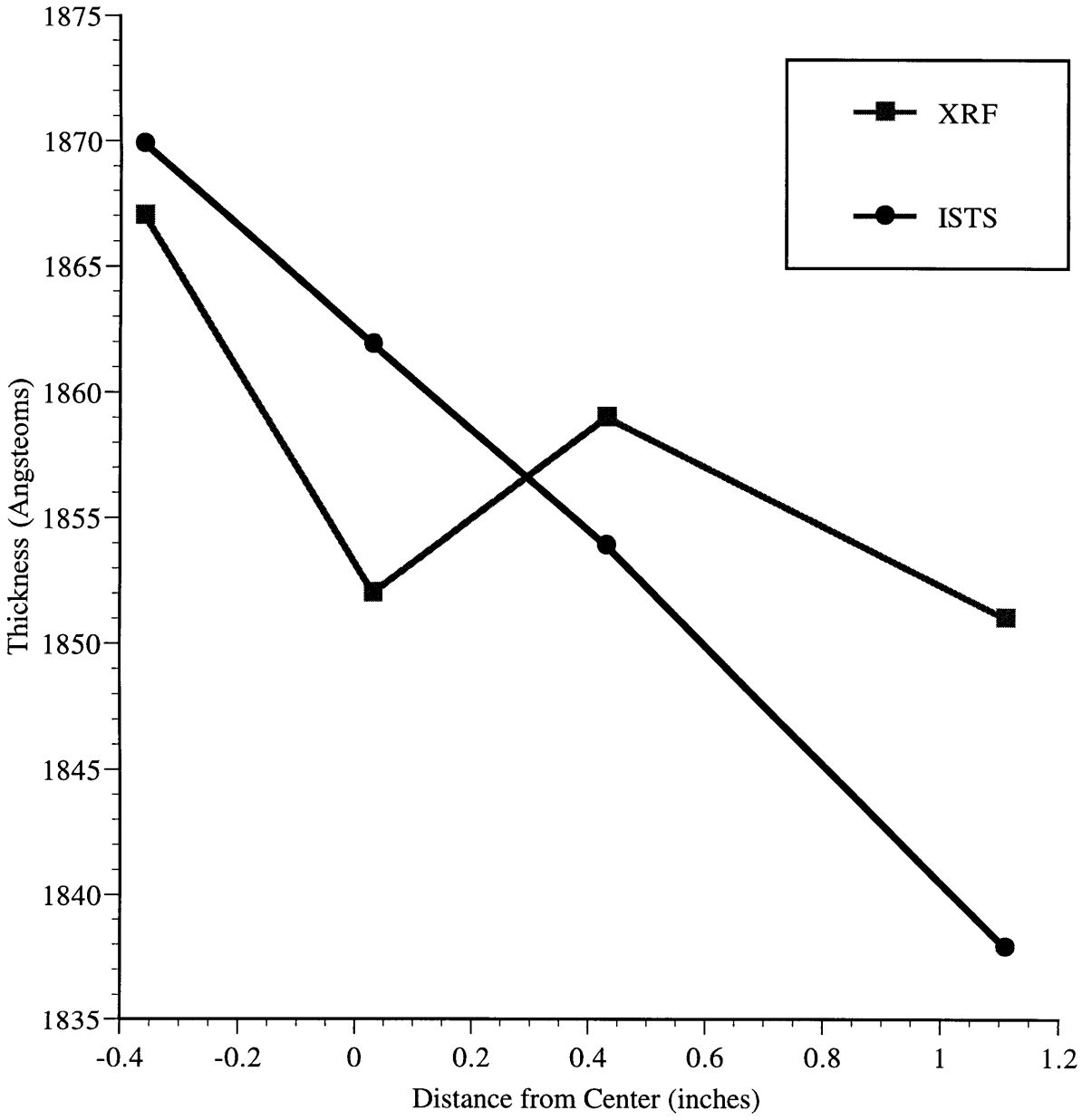

Figure 21: X-ray fluorescence (XRF) versus ISTS of nominal 1800-A Ti on 5000-A oxide on silicon. Measurements were made at several points across the wafer and are plotted as distance away from the center of the wafer.

technique to measure thickness and to assess the level to which the technique can address the specifications mentioned in Section 3.3.

For each set of samples, the acoustic frequency is plotted versus the varying film's nominal thickness value. The measurements were made at a range of wavevectors to investigate the varying response at different acoustic frequencies. In order to assess the precision of the measurement, which ultimately determines whether the technique will be useful as a metrology instrument, ten measurements were repeated on a single point. The standard deviation of acoustic frequency is converted to its corresponding thickness deviation based on the slope of the line. This error in thickness is reported on the frequency-thickness plot. The approximate slope of the line is reported in the figures. This slope represents the sensitivity of ISTS to thickness for that particular combination of thickness and wavevector. For the sake of simplicity, the plots of frequency versus thickness are only shown for two wavevector values. Figures 22-25 show frequency-thickness plots for single layer films on silicon substrates (Al, Ti, W).

Looking at the data for single layer films on silicon, there are two distinct trends that affect how the measurement can determine thickness. First, as the wavevector increases, the sensitivity of the measurement (change in frequency per change in thickness) and the measured frequency increase. Second, as the thickness of the layer being measured decreases, the sensitivity also increases. This means that theoretically the measurement should be made at as high a frequency as possible. In practice, the frequency attainable is limited by two things, First, the bandwidth of the detection system that is practical in a compact instrument is limited to about 1 GHz due to inherent limitations in the electronics. Second, exciting higher frequencies requires higher wavevectors. The wavevector is limited by the ability of the optics to cross the excitation beams at a large angle.

In practice, it is not always best to make measurements at as high a frequency as possible. The sensitivity of the measurement to changes in thickness may be increasing but the

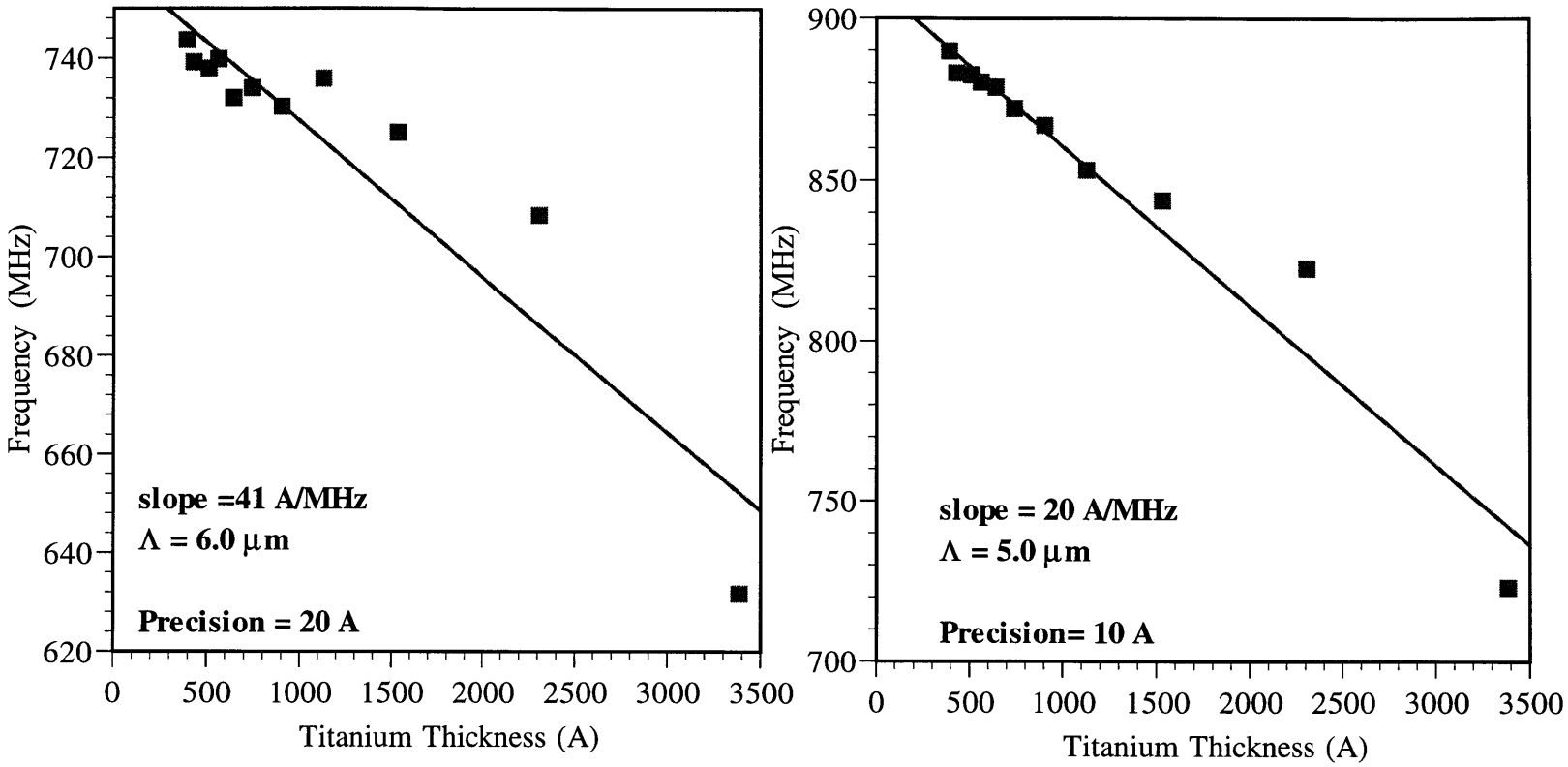

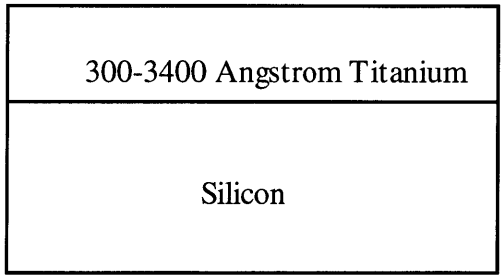

Figure 22: Frequency versus thickness plots at two different wavevectors for titanium films on silicon.

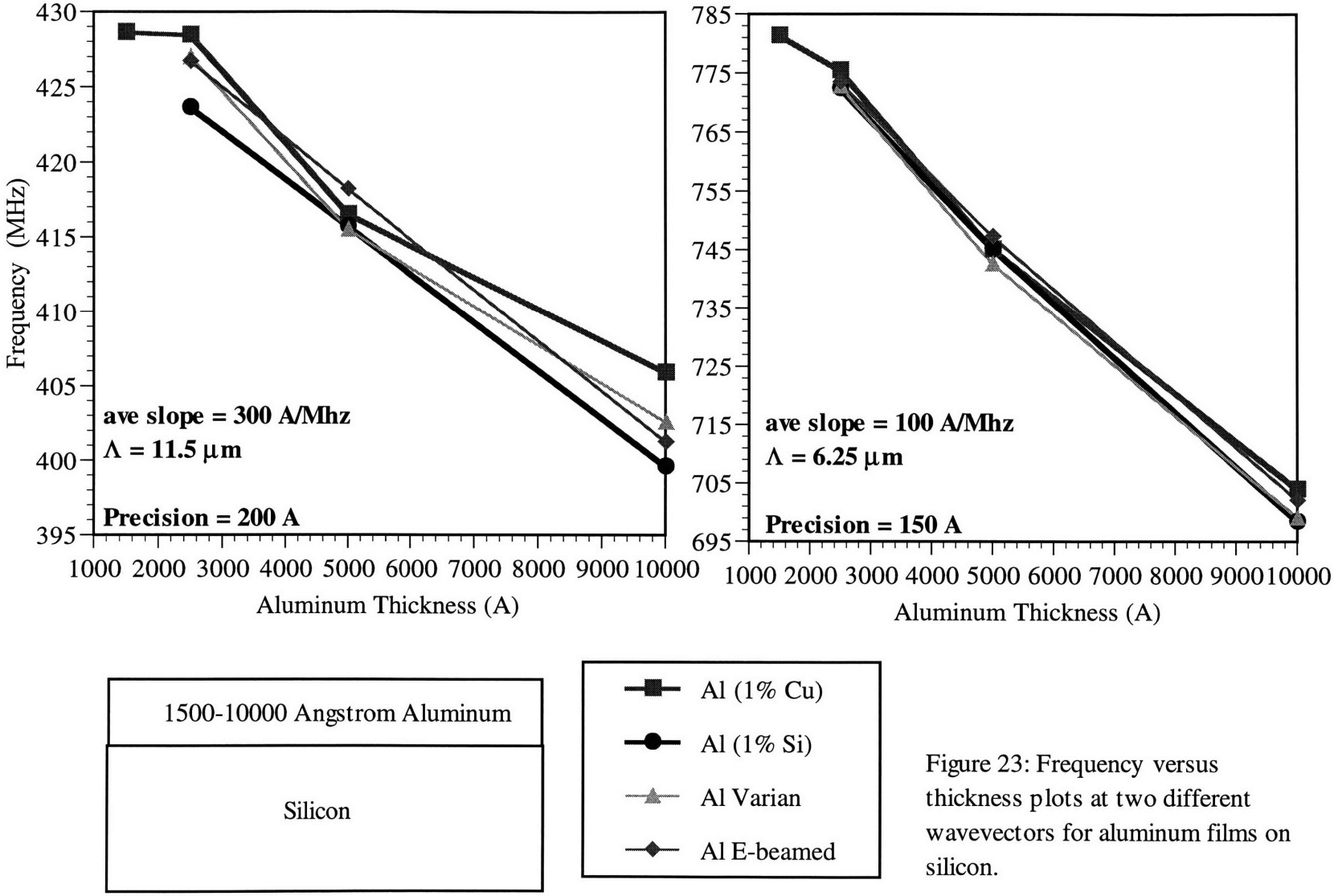

Figure 23: Frequency versus thickness plots at two different wavevectors for aluminum films on silicon.

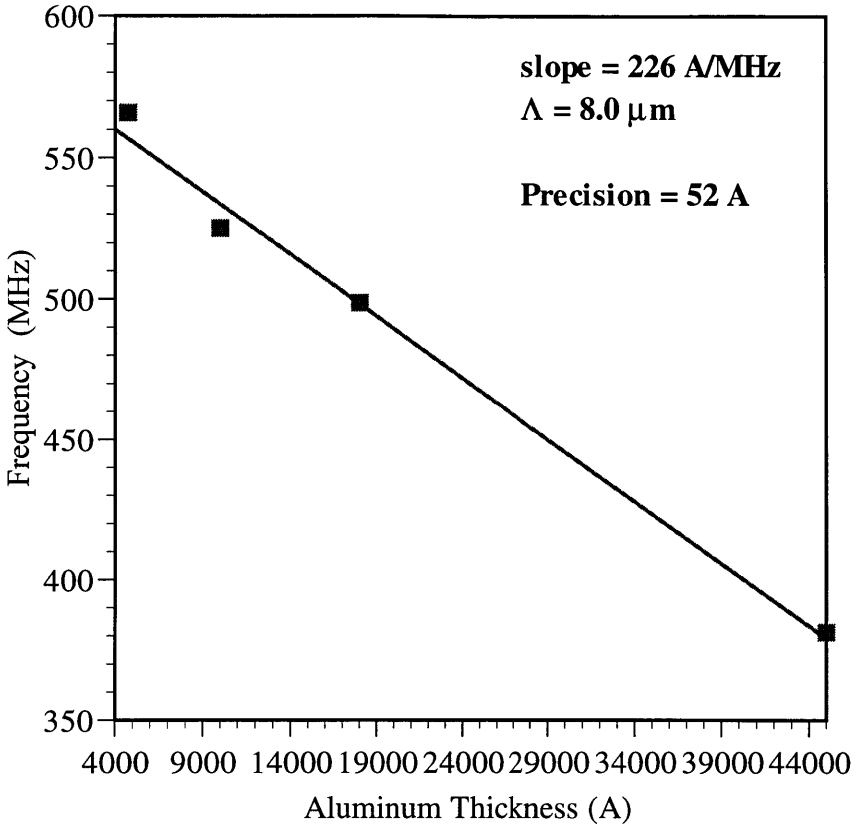

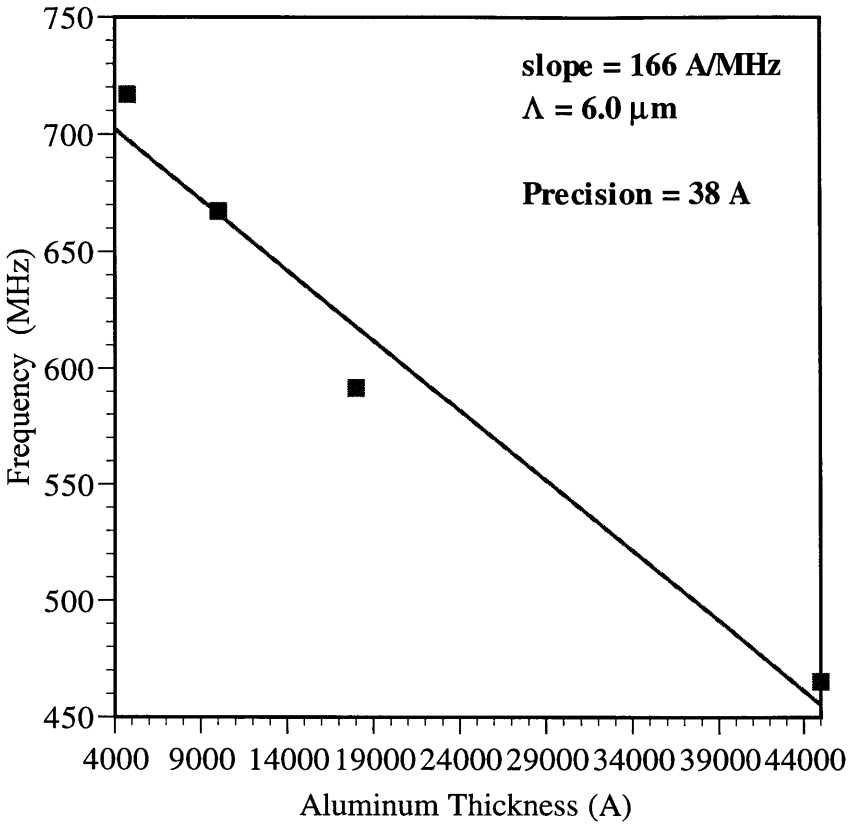

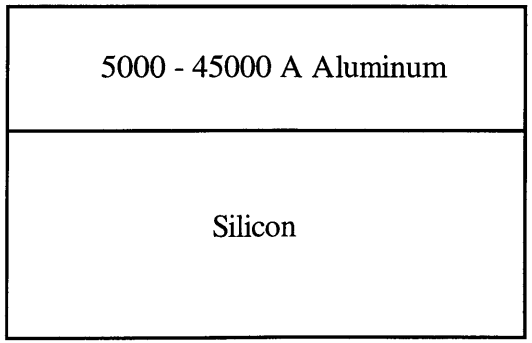

Figure 24: Frequency versus thickness at two different wavevectors for thick aluminum films on silicon.

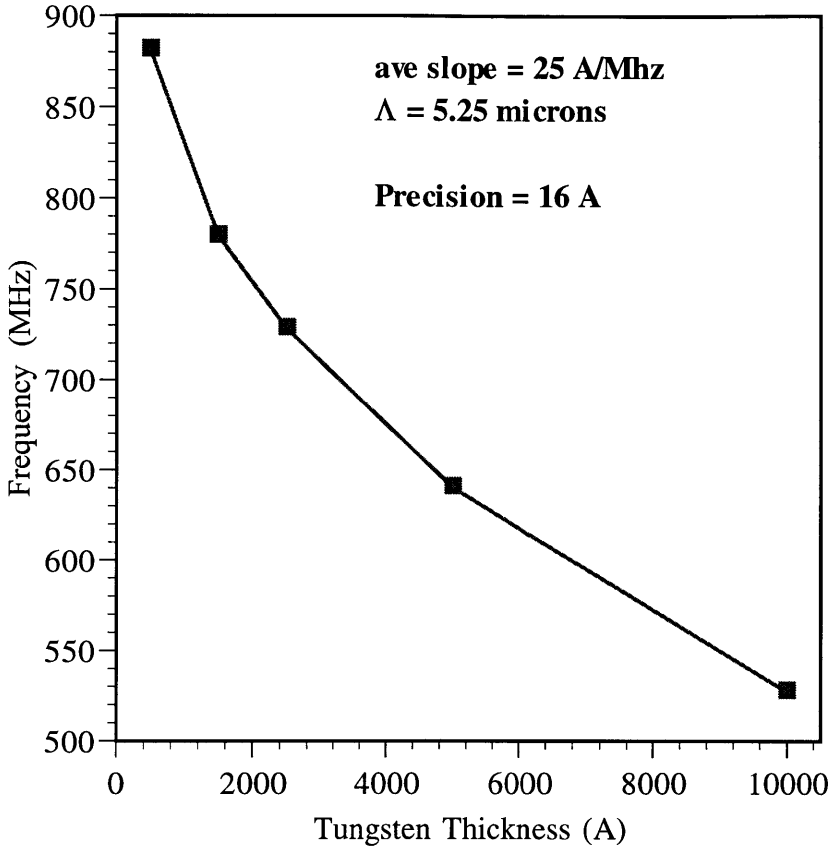

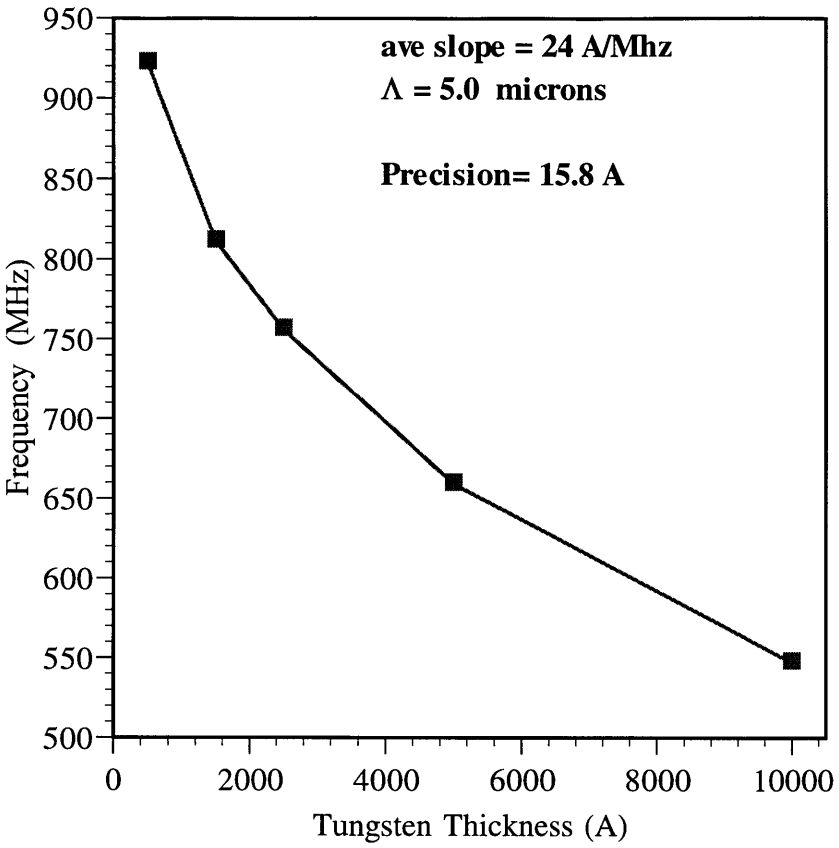

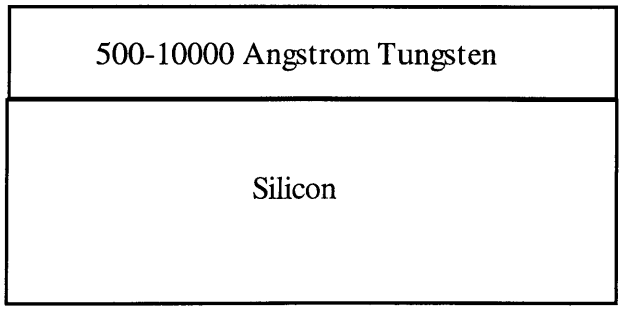

Figure 25: Frequency versus thickness at two different wavevectors for tungsten films on silicon.

resulting precision of the technique in resolving different thicknesses depends on the precision to which the frequency can be determined. As the acoustic frequency increases, the acoustic damping increases and therefore the precision to which the frequency can be determined deteriorates. There is therefore a tradeoff in going to higher frequencies between increasing sensitivity (larger change in thickness per change in frequency) and decreasing precision (higher standard deviation in frequency measurement translating to higher error in thickness determination). For most thin metal films that are of interest to the microelectronic community, acoustic frequencies between 400 MHz and 1GHz give the best results in terms of resolving thickness variations.

Also of interest to semiconductor manufacturers is the ability to measure the thicknesses of films in multilayer structures. For measuring underlying metal film thickness, two sample sets were analyzed. The first set (figure 26) contains a varying titanium:tungsten layer underneath a 2000-A aluminum top layer. These samples also contain a constant 1000-A oxide layer underneath the titanium:tungsten. The second set (figure 27) contains a varying underlying aluminum layer with a 500-A titanium:nitride top layer.

The data in figures 26-27 are summarized below in table 3, showing the best-case sensitivity and the best-case precision of ISTS measurement of metal film thickness in different ranges of thickness and structures.

Metal Layer	Thickness Range (A)	Sensitivity (A/MHz)	Precision (A)
Tungsten	10,000-2000	25	16
Ti:Tungsten (underlying)	1500-250	10	6
Titanium	2000-500	20	10
Aluminum	10,000-2000	100	150
	40,000-10,000	150	38
Titanium:Nitride	2000-500		50
Platinum[1]	2000-500		10
Cobalt[1]	2000-500		10
Niobium[1]	2000-500		10

Table 3: Sensitivity and precision results on various materials. [1] Estimated

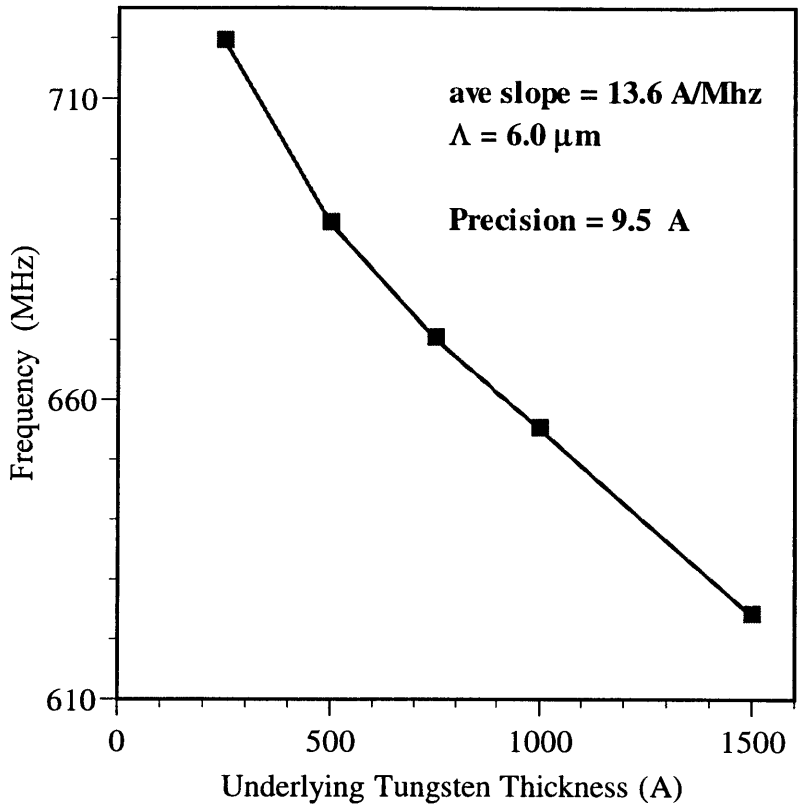

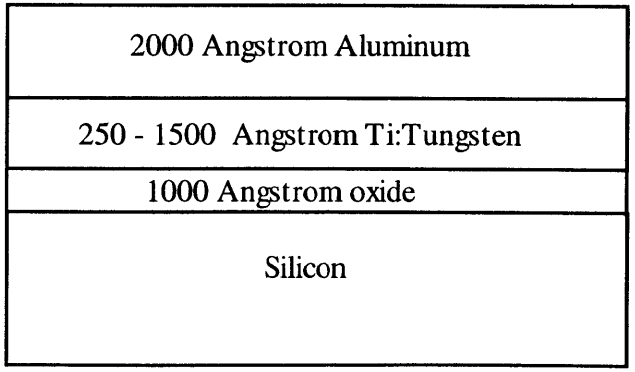

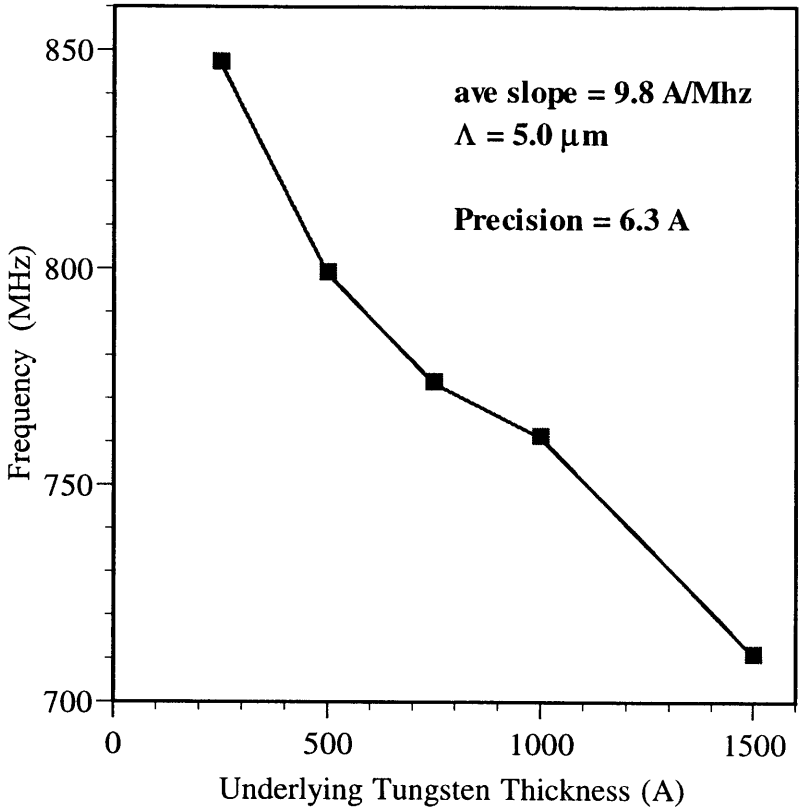

Figure 26: Frequency versus thickness at two different wavevectors for a varying Ti:W film underneath a 2000-A aluminum film and on top of a 1000-A oxide.

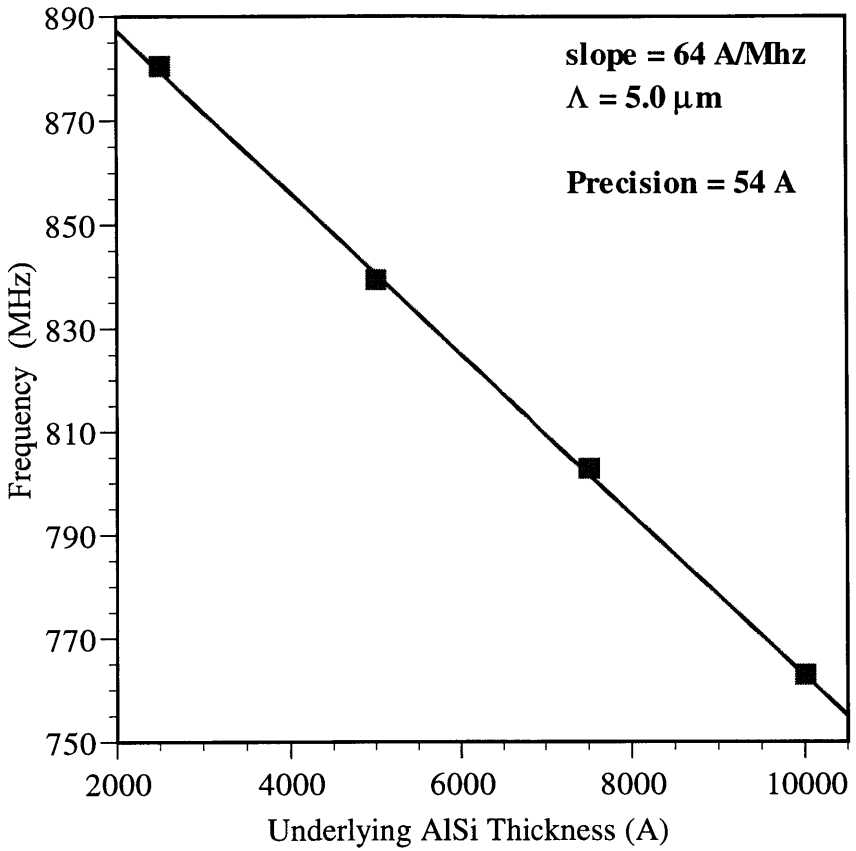

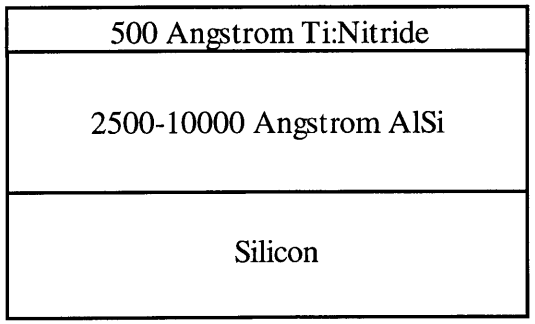

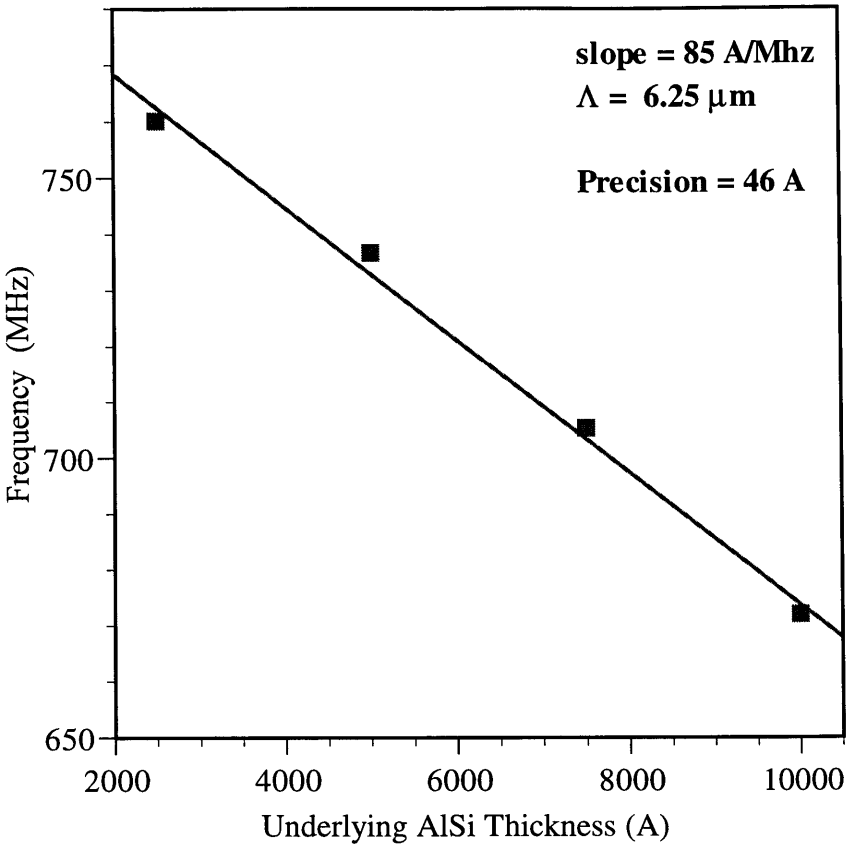

Figure 27: Frequency versus thickness at two differenct wvevectors for a varying AlSi film underneath a 500-A Ti:N layer.

3.6 Underlying Layer Thickness Determination

Table 3 demonstrates that ISTS is approximately ten times as sensitive to changes in tungsten thickness as it is to changes in aluminum thickness. Figure 28 shows a 49-point contour map made of an aluminum on tungsten structure. The frequency variation across the sample was assumed to be only due to thickness variations in the underlying tungsten because ISTS is more sensitive to these changes that to changes in the aluminum thickness. Therefore, the thickness contours on the plot represent changes in the underlying tungsten layer thickness and are consistent with other maps of tungsten layer thickness variations. The ability to determine underlying layer thickness is unique and valuable in a metrology instrument. The thickness of both layer could potentially be determined if the structure was probed at several different wavevectors.

3.7 ISTS Measurements Fit To Theoretical Dispersion Curves

The tungsten sample set was analyzed at approximately 10 wavevectors to compare the experimental data versus the theoretical model. When the data is plotted as acoustic velocity vs. the *qd* product using the nominal thickness values for d, the curve is not continuos. This indicates that the nominal thickness values do not indicate the correct ratios of actual thickness between the samples. In order to get a continous curve, the thicknesses were scaled as follows:

Nominal Thickness (A)	Scaled Thickness (A)
1500	1750
2500	2750
5000	4500
10,000	9000

The data as well as a best fit curve are plotted in figure 29. The parameters that are allowed to vary in the fit include the tungsten transverse velocity and the tungsten density (2519 m/s and 17.42 g/cc, respectively). The tungsten longitudinal value is fixed at the literature value of 5220 m/s [24]. The silicon substrate values are fixed as follows; density = 2.33 g/cc, longitudinal

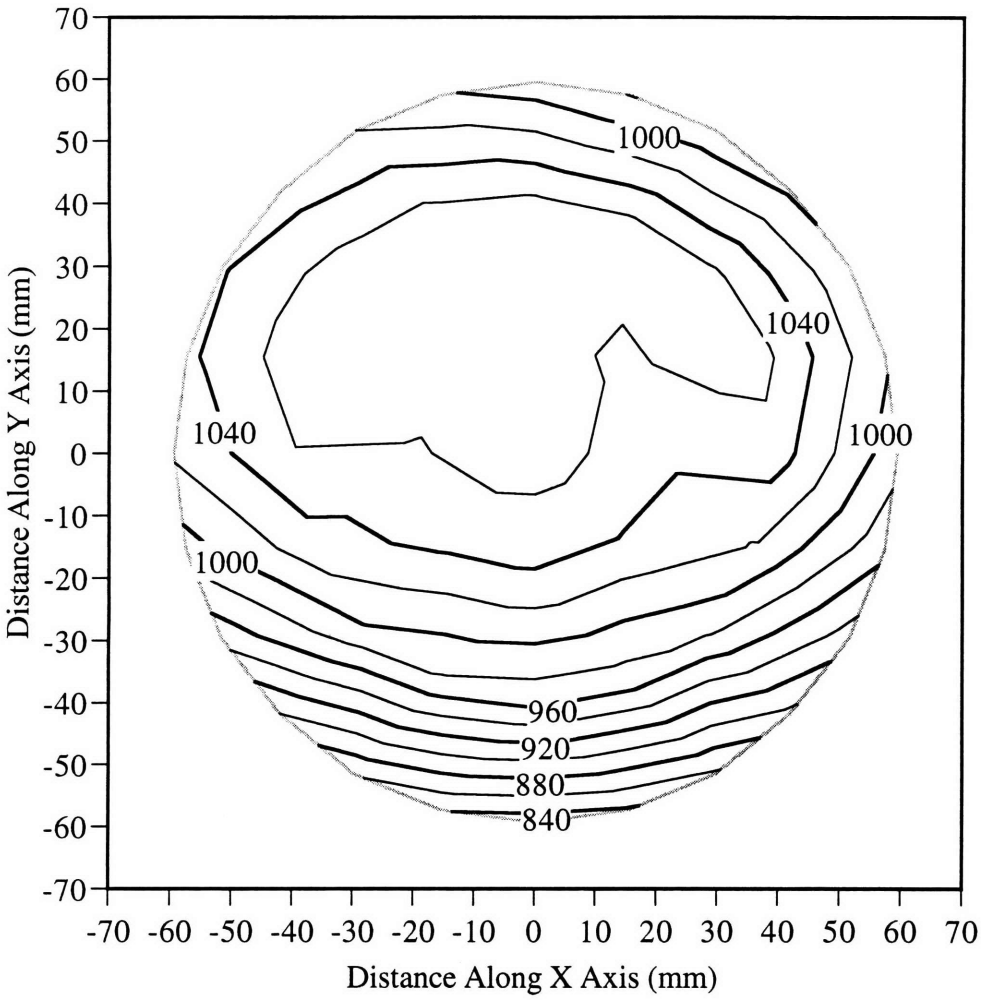

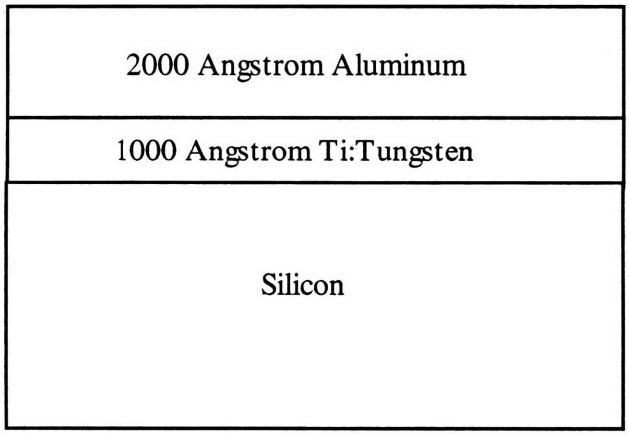

Figure 28: 49-point contour map showing variations in underlying Ti:W thickness as determined by ISTS measurements.

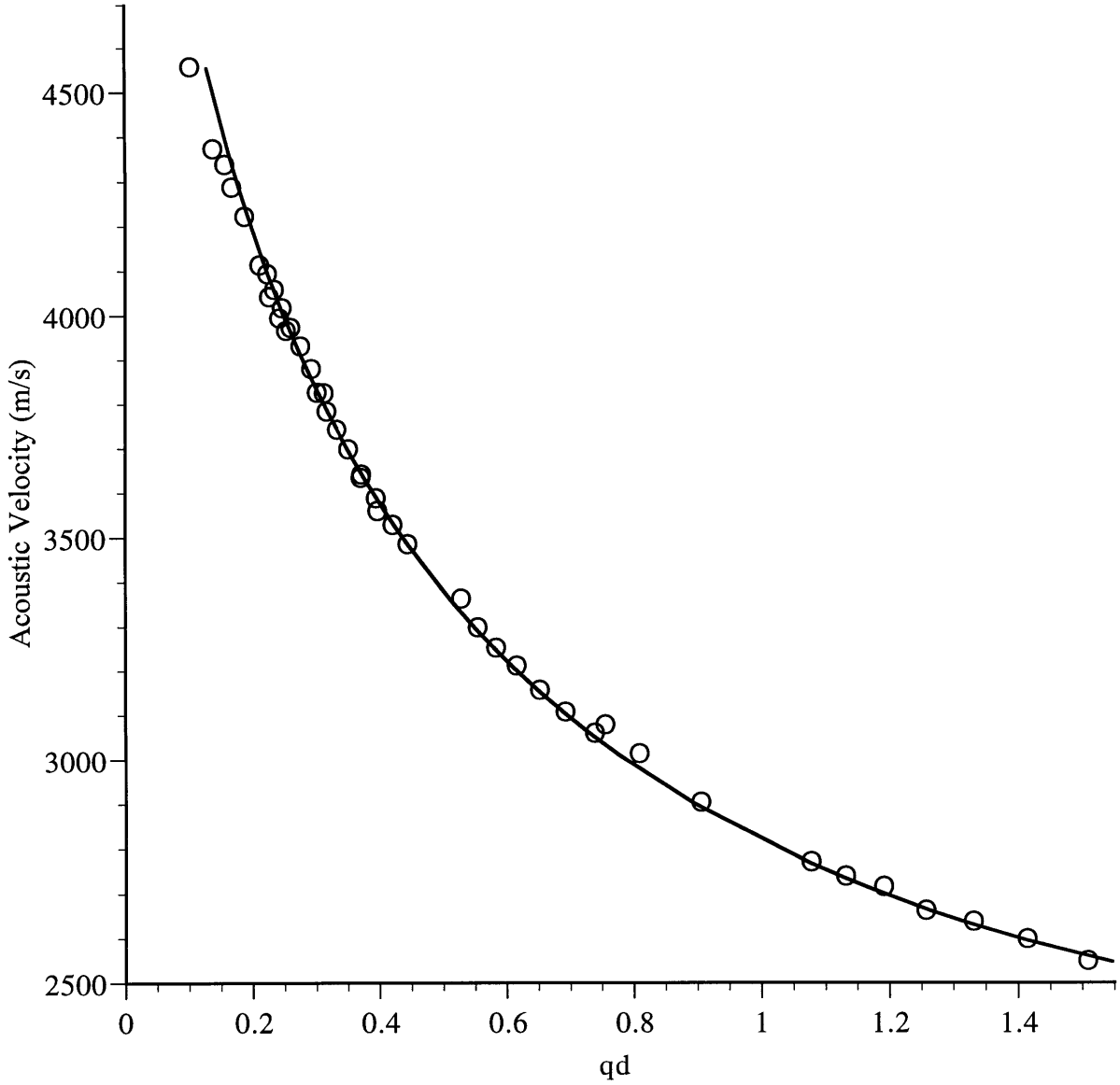

Figure 29: Best fit dispersion relationship for tungsten on silicon. Best fit parameters are: tungsten longitudinal velocity = 5220 m/s, tungsten transverse velocity = 2159 m/s, tungsten density = 17.42 g/cc, silicon longitudinal velocity = 9000 m/s, silicon transverse velocity = 5588 m/s, silicon density = 2.33 g/cc.

velocity = 9000 m/s, and transverse velocity = 5588 m/s. This assumes the density and modulus values are the same for all the films.

3.8 Repeatability

Research similar to what has been presented here is advancing at a very rapid rate because of the now commercial nature of the technique and the need to get results rapidly. Much effort has been put toward improving the precision of the measurement in order to achieve the goals set forth in section 3.3. Many ideas have been introduced to help reach this goal and some are described below.

Extracting a frequency from the acoustic oscillations seen in the data scans is a fairly straightforward process but room for improvement exists. Stronger signal level and a greater number of oscillations in the oscillatory data lead to a narrower power spectrum peak. The narrower the peak is, the easier it is to define the peak frequency value with less error. Therefore, methods to improve the signal level are one way to increase precision. Optimizing spot sizes and creating efficient diffraction conditions has increased signal levels by a factor of 5-10 since the data shown in this thesis were taken. This in turn has increased the thickness precision by a factor of approximately 1.5-3.

A second enhancement which has slightly increased precision is to fit the power spectrum peak to a Gaussian function. Up until now, the frequency was extracted from the FFT data by a peak-finding algorithm which simply finds the data point with the highest FFT power and records the corresponding frequency value. The ultimate precision this method can achieve is limited by the frequency difference between data points which is typically 0.2 MHz. Fitting the data points in the FFT data to a Gaussian function eliminates this limit in precision and speeds up the data processing because of the simple nature of the algorithm.

A third precision enhancement being investigated is the simultaneous excitation of multiple wavevectors. Special phase masks have been designed which cross three beams at the sample plane and excite two or more wavevectors. This in turn allows efficient excitation of two acoustic frequencies in the same time it takes to excite one frequency with two excitation beams. Extracting two frequencies from the time-domain data doubles the rate at which data can be taken. Increasing the rate at which data is acquired is an important consideration for a process control instrument. Figure 30 shows an example of data containing two acoustic frequencies excited at the same time. The frequency domain data (figure 30b) clearly shows two frequencies beating together. The low frequency peak is the difference frequency between the two modes.

In developing any new technique which measures a material parameter in a new way, an important question to ask is how repeatable the measurement is. A technique can be shown to be sensitive to a property which is valuable to measure, but unless the technique can repeat that same measurement several times in succession and return the same value, it will not be beneficial.

In order to determine the repeatability associated with the ISTS measurement and to make sure that variations measured at different points across wafers were reproducible, measurements were made at a series of spots, reached by an automated x-y stage, several times in succession and measurements were repeated at the same spot on a wafer several times in succession. For most materials, the uncertainty in acoustic frequency in a single measurement is less than ±1 MHz. The amount that the film thickness varies with acoustic frequency depends on the details of the film-substrate assembly, but typically this corresponds to a thickness uncertainty of less than ±50 A and can be as low as ±5 A in a film made of a dense material such as tungsten. These results have been presented in more detail in section 3.5. In demonstrating the repeatability of contour maps, this precision error is combined with the positional error of the stage. To demonstrate this repeatability, the points are plotted in succession instead of in a map

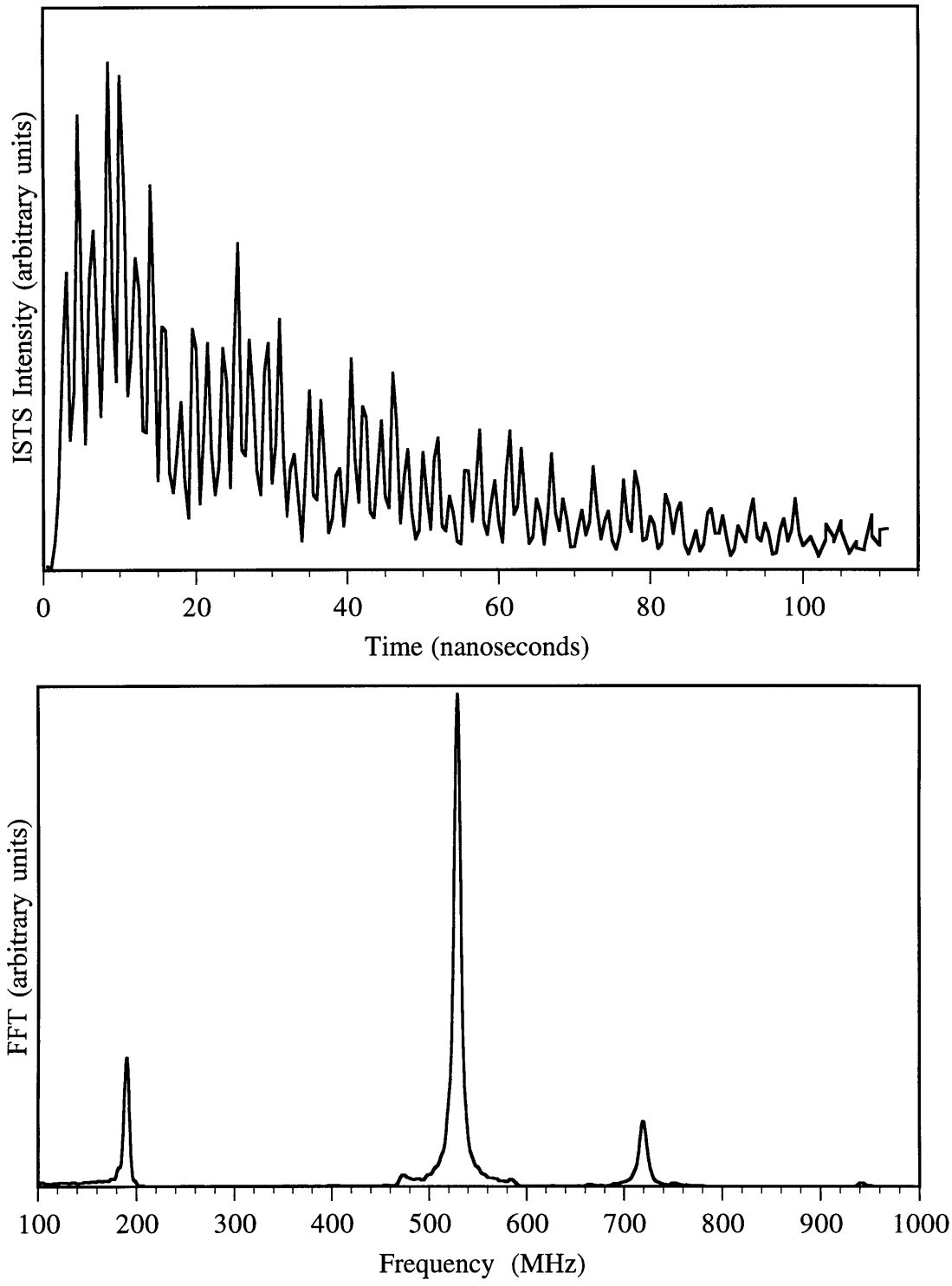

Figure 30: (a) ISTS signal from 4000 Å niobium on 5000 Å oxide on silicon. (b) Power spectrum from data in (a). The two higher frequencies represent two different modes which are 529 MHz and 720 MHz. The low frequency peak is an artifact of the FFT algorithm and gives the difference between the two higher frequencies (191 MHz).

form (figure 31). This allows each individual point to easily be compared from the first scan to the second scan. Repeatability is apparent as the points from scan 1 and scan 2 line up very closely.

3.9 Sensitivity Analysis

The results in section 3.5 very clearly demonstrate the precision of the ISTS technique with respect to instrument response. In some applications of the technique for determining metal film thickness, a calibration curve can be made with samples of known thickness and constant mechanical properties. Then, unknown samples can be examined and the thickness accurately determined. In other cases, however, it is desirable to have an instrument for which no calibration sample set is needed. Instead, the details of the structure (underlying layer thicknesses and mechanical properties) are entered into an algorithm which then outputs a thickness for the unknown layer. This presents some challenging problems in terms of accuracy which are discussed below.

In general, the ISTS result is sensitive to subsurface structure extending into the sample a distance on the order of the acoustic wavelength Λ, which typically is adjusted within the 1-10 micron range. Small deviations in subsurface layer thickness or modulus from their assumed values have relatively minor effects on the film thickness values calculated based on the thermoelastic equations of motion, but nonetheless need to be understood. Table 4 gives several examples of how errors in the assumed thickness of an underlying oxide layer affects the thickness value calculated for a top metal layer. The oxide thicknesses assumed are 1000 A or 5000 A for each structure as these are typical thicknesses of oxide layers that are used. The metal thicknesses used are representative examples for these metals. The calculations are done first assuming that the oxide thickness is 5000 A or 1000 A and then assuming they are 10%

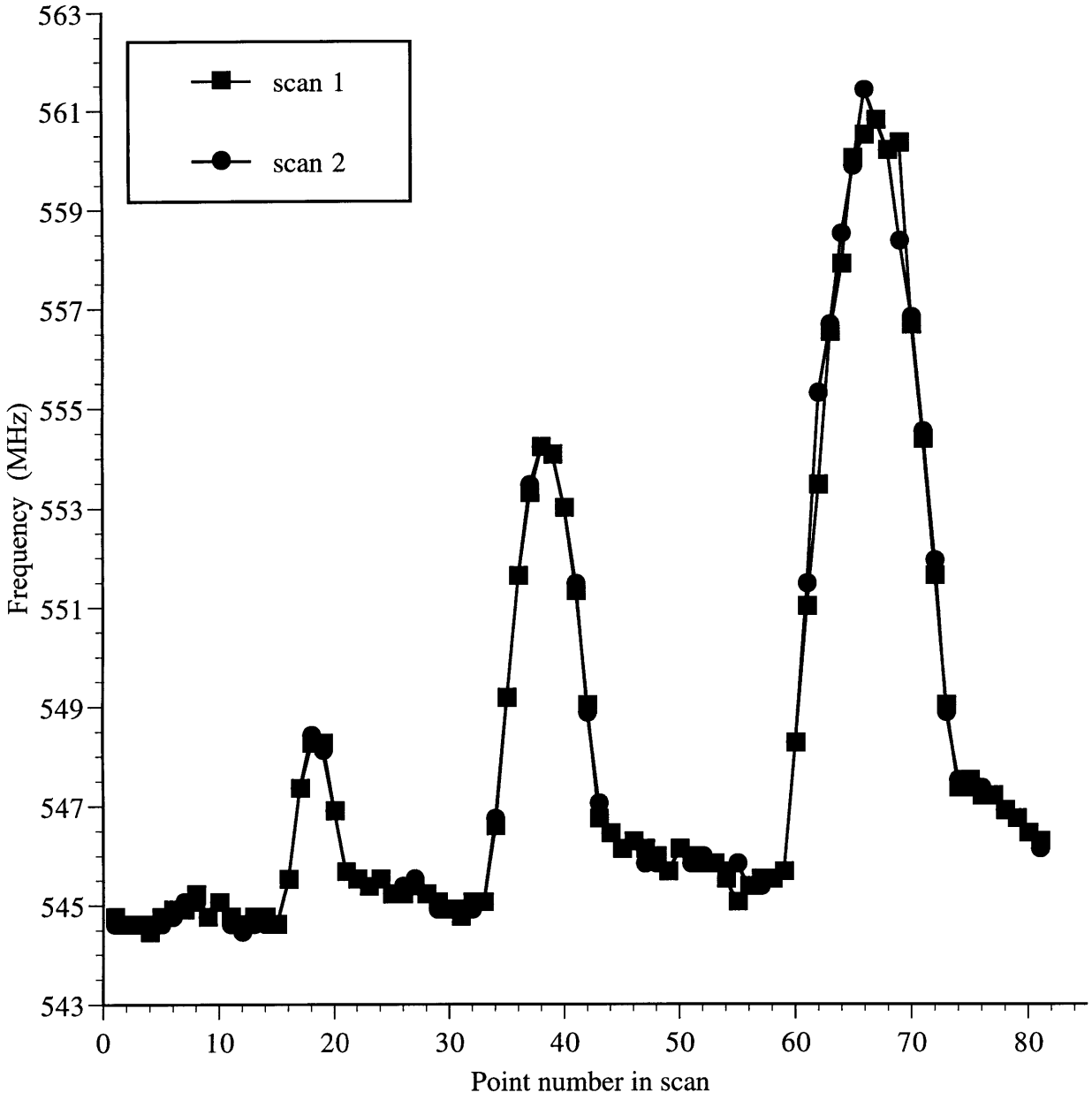

Figure 31: ISTS measurements on a 10,000-A tungsten film on silicon plotted to demonstrate point-to-point repeatability. X-axis represents point number in an 81-point contour map.

lower. The results demonstrate the error in the calculation of the metal thickness if the oxide thickness assumed for the calculation is 10% different than the actual oxide thickness.

Metal	Assumed Oxide (A)	Calculated Metal (A)	Actual Oxide (A)	Recalculated Metal (A)	% error in Metal
Titanium	5000	2000	4500	2183	9.2
Titanium	1000	2000	900	2015	0.8
Aluminum	5000	8000	4500	8419	5.2
Aluminum	1000	8000	900	8086	1.1
Tungsten	5000	5000	4500	5089	1.8
Tungsten	1000	5000	900	5019	0.4

Table 4: Effects of uncertainties in subsurface oxide thickness on metal layer thickness deduced from ISTS data.

The result depends on the wavevector the measurement was made at and also on the materials and thicknesses in the structure. For the calculations above, the result is for the wavevector value, q, of 1.5 μm^{-1} (Λ=4.1 μm). As expected, the higher the metal to oxide thickness ratio, the less sensitive the structure is to errors in subsurface layer thickness.

Similarly, table 5 shows errors that result from wrong assumptions of the film and substrate elastic constants and density. The table shows two films (5000 A tungsten and 8000 A aluminum) with and without a 5000-A oxide layer underneath, both on a silicon substrate. The columns show the calculated thickness (and percent error from actual) if a value that is 5% higher than actual is used for either the density, longitudinal velocity (V(l)) or transverse velocity (V(t)) of either the film itself or the silicon substrate.

Top Layer	Oxide	Silicon			Metal		
	(A)	ρ + 5%	V(l) + 5%	V(t) + 5%	ρ + 5%	V(l) + 5%	V(t) + 5%
5000-A W	5000	5163 (3.3%)	5326 (6.5%)	5032 (0.6%)	4590 (-8.2%)	5050 (1.0%)	5040 (0.8%)
5000-A W	0	5324 (6.5%)	5693 (14%)	5105 (2.1%)	4638 (-7.2%)	5089 (1.8%)	5045 (0.9%)
8000-A Al	5000	8245 (3.1%)	8635 (7.9%)	8065 (0.8%)	7405 (-7.4%)	8219 (2.7%)	8266 (3.3%)
8000-A Al	0	8378 (4.7%)	9310 (16%)	8225 (2.8%)	7610 (-4.9%)	8363 (4.5%)	8317 (4.0%)

Table 5: Effects of uncertainties in metal and substrate mechanical properties on layer thickness deduced from ISTS data.

These results again demonstrate the sensitivity the measurement has to subsurface structure.

Another potential source of error in the accuracy of the model to determine film thickness could arise from residual stress in the films due to processing. In a previous study, Rogers and Nelson [9] determined residual stress in unsupported polyimide films. In these unsupported films, the lowest order mode is sensitive to residual stress only at very low wavevector times thickness products (*qd*). Rogers and Nelson concluded that there are no modes in supported films which would show an enhanced sensitivity to residual stress and small spot-to-spot variations in the ISTS response frequency due to inhomogeneities will tend to wash away any resisual stress effects. In addition, metal film thickness determination is optimized at high wavevector values where residual stress has virtually no effect on the measurement.

A second source of error which turns out to be affecting the precision and accuracy of the technique is the positional error of the sample on the optical axis. Figure 32 shows the dependence of the measured acoustic frequency at the exact same point on the position of the sample along the optical axis (z-axis). The variation is on the order of several MHz for a 100μm change in z. This change in frequency corresponds to an error in thickness up to several hundred angstroms, which limits the precision of the measurement if the sample cannot be repeatedly placed at the same position along the z axis.

It is believed that the reason the frequency measurement changes with z is that the spatially periodic interference pattern created by the two intersecting beams is not constant along the optical axis. This creates a systematic variation in the grating pattern, hence a systematic variation in the wavevector. This gradient in the wavevector along the z-axis is what account for the change in frequency along the z-axis.

There are several key aspects to the design of the compact instrument which allow for corrections to this problem to be made. In order to make the experiment function properly, the two excitation beams and the probe beam must overlap in space at roughly the same point. This "fixes" where the sample must be in z to a certain extent but still allows efficient excitation and

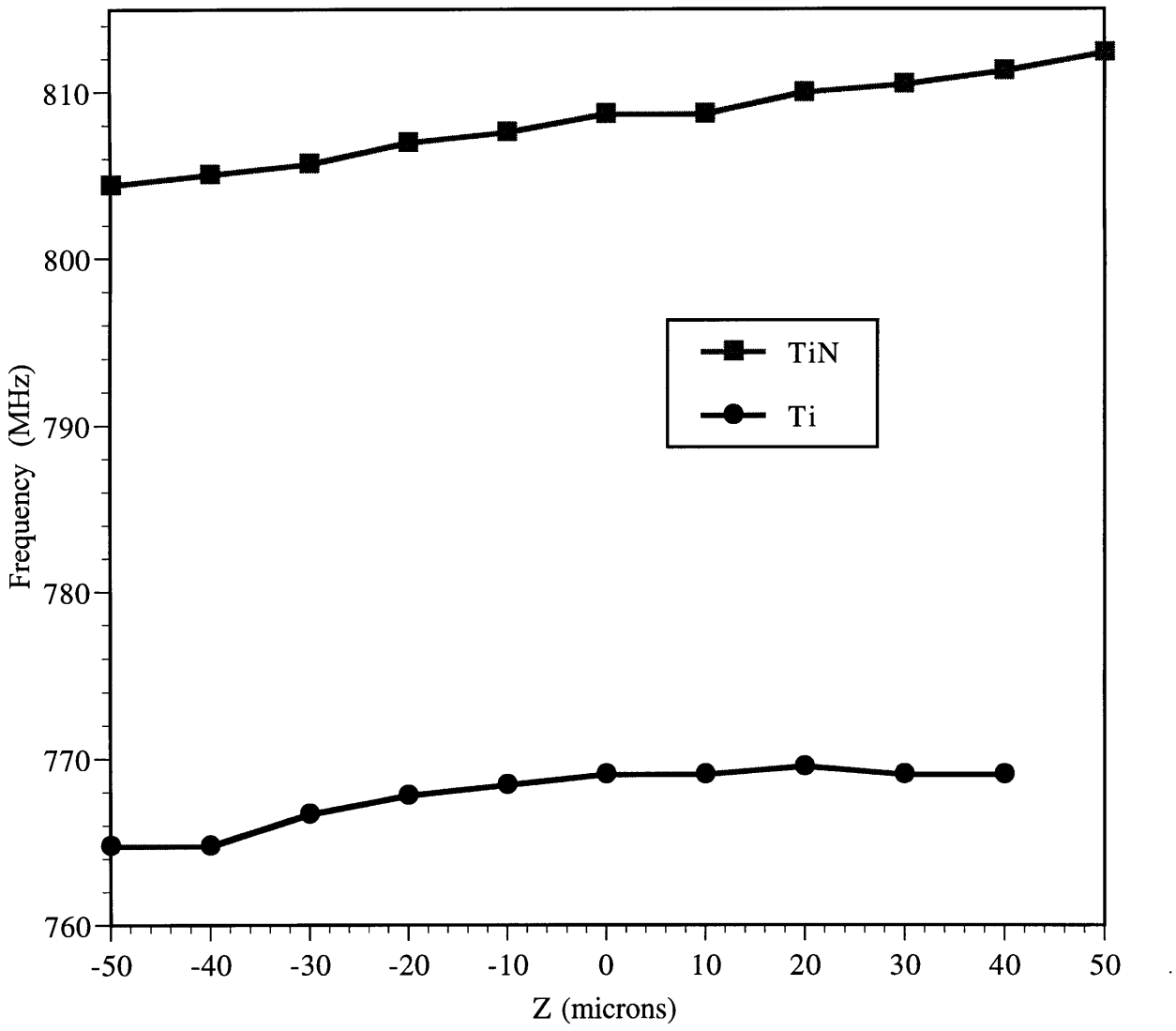

Figure 32: Frequency variation as a function of position along the optical axis for titanium and titanium:nitride.

detection of acoustic waves over a range z. As the sample is moved along z away from the optimum, the probe beam begins to sample a spot on the diffraction grating that is farther away from the center of where the excitation beams cross. This leads to less efficient diffraction and therefore a weaker signal. A second effect which hinders achieving the optimum signal level is the fact that the photodetector is fixed in space and detects the diffracted signal best when the sample is at the optimum z. These two effects of varying z on the efficiency and strength of the signal diffraction can be measured by observing the peak height in the FFT which is a direct reflection on the strength of the signal. If the peak height is plotted versus z, a Gaussian shape emerges which has at its peak the best signal level and hence the optimum z. An "autofocus" routine has been implemented in the user interface which records the FFT power as a function of z, fits a Gaussian shape to the data points, and moves the sample to the optimum z for data collection.

A second solution to the variance of the wavevector with z being approached is to redesign the optics so that there is no variation of the grating pattern with z. This can be achieved through appropriate use of lenses to minimize the divergence of the grating pattern at the sample plane.

A method of improving accuracy currently being installed in the compact instrument is an internal wavevector calibration standard. The method for wavevector calibration currently used is to calibrate thickness values to other techniques. This method is not completely reliable as there are several other variables (i.e. mechanical properties) which are not known accurately and can affect the wavevector calibration. By measuring a bulk material with known mechanical properties, an accurate value for the wavevector can be determined. The calibration standard will reside in the sample plane at a point that can easily be reached by the automated x-y stage at any time during instrument operation. The bulk material being sought is one which is very inert

to the atmosphere over long periods of time as adsorption of gases and formation of thin oxide layers can affect the ISTS measurement of the standard.

3.10 Conclusions

ISTS measurements of opaque film thickness have been conducted on a variety of film-substrate assemblies. Capabilities for film thickness measurement and two-dimensional mapping of wafers has been demonstrated. Comparison between ISTS results and the results of conventional measurements including stylus profilometry, SEM, and 4-point resistance probing was carried out to validate the ISTS measurement method against widely used alternatives. Among these methods, only ISTS offers rapid, non-contact, non-destructive evaluation of opaque film thickness. Implications of precision and accuracy have been analyzed as they are important considerations in the development of ISTS as a robust technique.

Chapter 4: Method For In-situ Evaluation of Radiation-Induced Hardening of Polyimide Films

4.1 Introduction

All the measurements discussed previously are aimed at application in microelectronics. However, the ISTS method has application in a wide range of other areas. One such example follows.

Magnets used to confine plasma in fusion reactors at the International Thermonuclear Experimental Reactor (ITER) will experience extreme operating conditions. The magnets are operated at 4.2 K and are exposed to high fluences of fast-neutron and gamma irradiation as well as shear and compressive forces. The sensitivity of the magnet insulation material to these operating conditions is a critical feature of the magnet performance. In particular, degradation of the mechanical properties of magnet insulation upon fast-neutron and gamma irradiation must be assessed throughout the projected 25-year lifetime of the magnet. One such magnet insulation is a hybrid consisting of a barrier or coating in combination with vacuum-pressure impregnation and prepreg primary insulation [25]. The barrier layer in this hybrid system can be a polyimide film.

In this study, ISTS was used to determine viscoelastic and thermal transport properties of DuPont Kapton film before and after neutron irradiation to assess the degradation of the mechanical properties that would be expected to occur in a nuclear reactor environment. Furthermore, it is shown that ISTS could be used as a non-contact, non-destructive monitoring device providing continuous feedback of the insulation material performance over the lifetime of the magnet.

Impulsive stimulated thermal scattering, or ISTS, is an all-optical method for non-contact, non-destructive, real-time measurement of mechanical and physical properties of thin film materials [11,14,15]. Two subnanosecond excitation laser pulses are spatially and temporally crossed at the surface of an absorbing sample to form an optical interference or "grating" pattern. Optical absorption and sudden spatially periodic heating give rise to thermal expansion and acoustic responses at the grating wavevector. The wavevector is a function of the crossing angle and the wavelength of the excitation light pulses. The thermal and acoustic responses of the material cause a spatially periodic modulation or "ripple" of the sample surface and can be monitored through time-dependent diffraction of a quasi-cw probe beam.

4.2 Experimental Setup - Laboratory Version

The ISTS experimental setup has been described elsewhere [14,15] and is shown in figure 33. Frequency-tripling of the output of a Q-switched, mode-locked and cavity-dumped Nd:YAG laser yields 355-nm excitation pulses of 100 picoseconds duration with 10 μJ of energy. This wavelength matches the red edge of the polyimide electronic absorption spectrum, and strong absorption leads to efficient heating. The pulses are split with a 50% reflector and recombined at the surface of the sample at an excitation angle, θ_E, which was 3.39° in this study. The probe beam is the electro-optically gated output of a cw single-mode argon ion laser which produces 1W at 514 nm with a flat intensity profile. The gate gives rise to a quasi-cw square pulse with an adjustable temporal window. The diffracted signal is detected in reflection mode and temporally analyzed using a high-bandwidth amplified photodiode and digitizing oscilloscope. The apparatus used for this experiment occupies an area of about 4 ft x 8 ft and requires specialized electrical power, cooling water, and technical expertise on the part of the operator. As demonstrated in the section on metal film thickness, the technique can be packaged

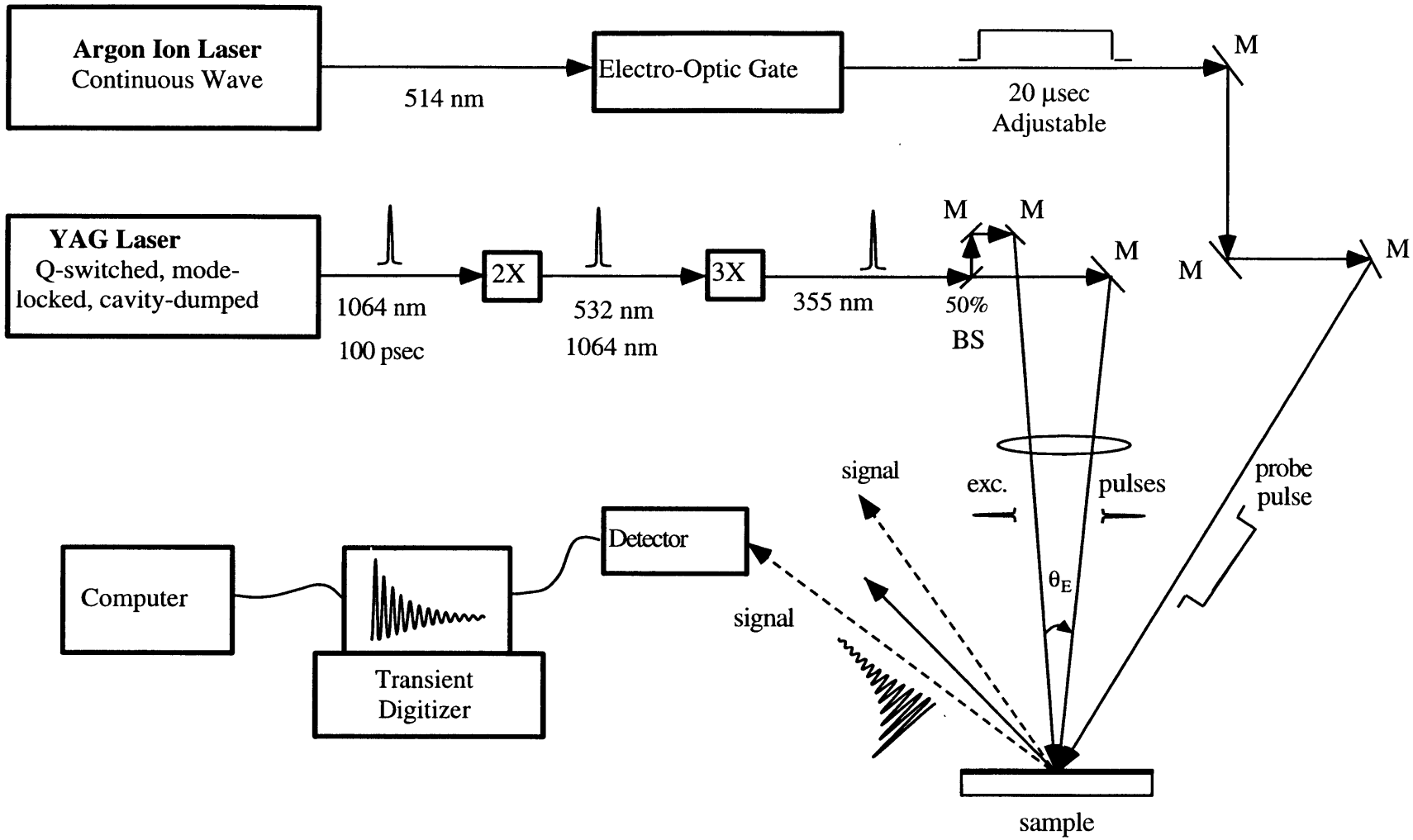

Figure 33: ISTS experimental setup for thin films. Excitation wavelength, λ_e=355 nm.

in a simplified, compact manner using solid-state lasers and an optimized beam-delivery system. This would allow ISTS to make measurements *in-situ* on insulation materials.

Two DuPont polyimide samples, Kapton H and Kapton HA [26] films of 12.5 mm diameter and 0.25 mm thickness, were used. The films were held at 4.2 K and irradiated in a nuclear reactor with a fast-neutron fluence (E>0.1 MeV) of 3.1×10^{22} n/m^2. The gamma dose and the total dose were 3.6×10^7 and 6.7×10^7 Gy, respectively. Irradiated films and unirradiated control samples were examined with ISTS in order to determine the effects of irradiation on the films and on the ISTS signal.

4.3 Results

Typical data from irradiated and unirradiated Kapton H are shown in figure 34. The data shown are the average of 500 single-laser-shot data scans and were collected in 5 seconds. Figure 34a shows acoustic oscillations which gradually damp away on nanosecond time scales. Figure 34b shows the same data on a microsecond time scale and a logarithmic signal intensity scale. The long-time signal is due to steady-state thermal expansion which washes away due to thermal diffusion from the peaks to the nulls of the grating. The data can be fit to the following expression [14]:

$$I(t) \propto |\Delta\rho(t)|^2 = [Ae^{-\Gamma t} - Be^{-\gamma t}\cos(\omega t)]^2$$

where $\Delta\rho$ is the peak-null density excursion. This represents the square of the material displacements giving rise to diffraction. The first term describes the steady-state thermal expansion response with amplitude A and thermal diffusion rate Γ, and the second term describes the transient acoustic response with amplitude B, acoustic damping rate γ, and acoustic frequency ω. A fourier transform of the data in figure 34a is shown in figure 34c. This figure shows that the acoustic responses of the film before and after irradiation are dominated by a single mode at

approximately 150 MHz. From the acoustic information provided through ISTS, sound velocities and elastic loss moduli can be determined. From the thermal decay rate, the thermal diffusion can be deduced.

There are three distinct differences between data from the irradiated and unirradiated samples. Figure 34b reveals a significant increase in the thermal decay time (or a decrease in the thermal diffusion rate) upon irradiation. Figure 34a shows a shift toward higher acoustic frequency and damping rate upon irradiation. Figure 35 shows the results for Kapton HA, which exhibit the same trends. Table 6 summarizes the effects of irradiation on acoustic frequency, thermal decay rate and acoustic damping rate of Kapton H and HA as derived from these figures.

Status	Material	Acoustic Frequency $\omega/2\pi$ (MHz)	Thermal Decay Rate, Γ (μs^{-1})	Acoustic Damping Rate, γ (μs^{-1})
control	Kapton H	148.3 ± 0.4	0.96 ± .07	15.3 ± 0.8
irradiated	Kapton H	151 ± 3	0.78 ± .04	34 ± 6
control	Kapton HA	149.2 ± 0.5	0.95 ± .10	17.2 ± 1.0
irradiated	Kapton HA	159 ± 2	0.79 ± .05	27 ± 4

Table 6: ISTS data obtained from Kapton H and HA polyimide films before and after irradiation. Note: Data in table are the averages of 10 spots per sample. Error shown is ± 1 standard deviation.

Previous studies of radiation-induced effects in Kapton have been performed using X-ray diffraction, dynamic viscoelasticity, and tensile testing measurements [27]. X-ray diffraction reveals that irradiation leads to disordering of the amorphous Kapton HA and partially crystalline Kapton H structure. In particular, a partially crystalline Kapton H structure (25% crystalline, 75% amorphous) is converted into a fully amorphous structure during irradiation. Dynamic viscoelasticity measurements show that in both Kapton H and HA, the glass transition temperature T_g increases following irradiation, with the change in Kapton H being much larger than in Kapton HA. The increase in T_g indicates that structural changes during irradiation consist predominantly of crosslink formation. Crosslinking causes greater constraints among the molecules and decreases the mobility of amorphous chain segments. Mechanical testing shows

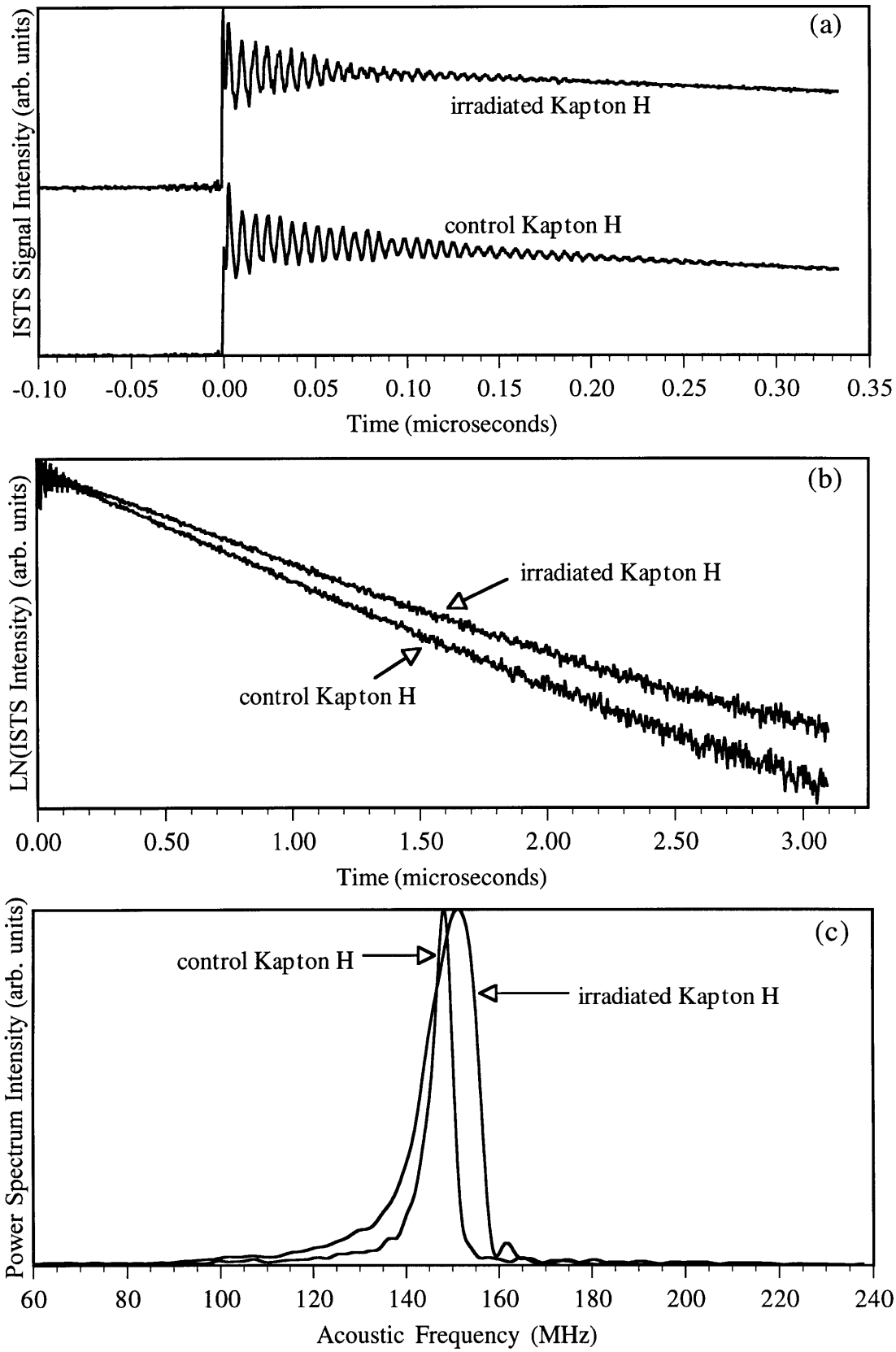

Figure 34: (a) ISTS data from control and irradiated Kapton H samples. (b) Same data as (a) on a longer time scale and a logarithmic intensity scale. (c) Power spectra of data in (a).

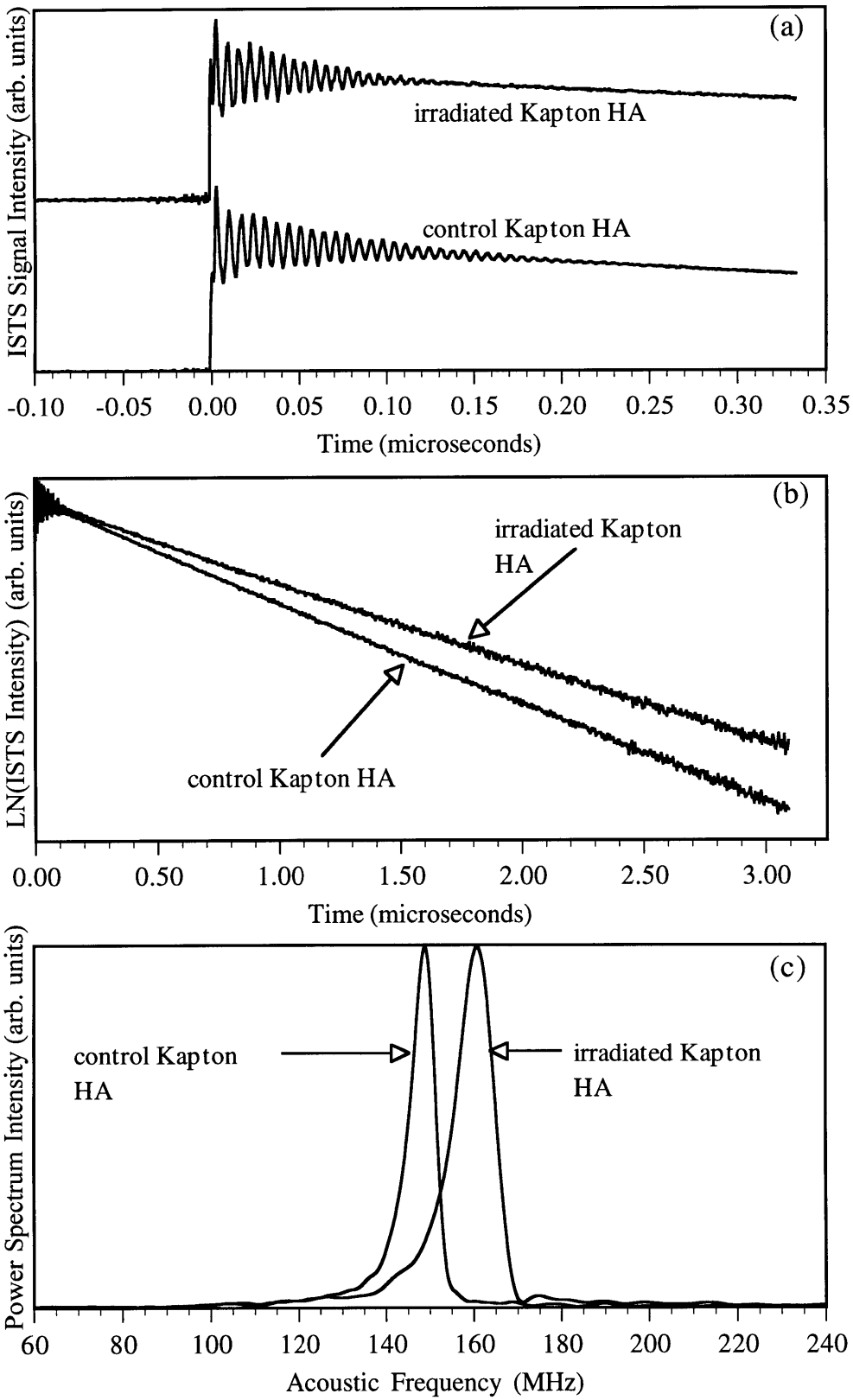

Figure 35: (a) ISTS data from control and irradiated Kapton HA samples. (b) Same data as (a) on a longer time scale and a logarithmic intensity scale. (c) Power spectra of data in (a).

that irradiation increases microhardness, tensile modulus and yield strength of both Kapton H and HA. These results are consistent with the hypothesis that crosslink formation as opposed to bond scission is the main damage mechanism during irradiation. Irradiation decreases the total strain to fracture of both Kapton H and HA. The reduction of total strain to fracture (a measure of radiation-induced hardening) is shown to be larger in Kapton H than in Kapton HA.

The ISTS results showing an increase in acoustic frequency in both Kapton H and HA upon irradiation indicate an increase in modulus, consistent with the earlier conclusions. The increase in acoustic damping rate in Kapton H and HA can be explained in terms of increased disorder which results in increased scattering of acoustic waves. As shown in table 6, the increase in acoustic damping rate and the corresponding increase in disorder is higher in Kapton H than in Kapton HA upon irradiation. This result is consistent with the earlier conclusions that total strain to fracture, as a measure of radiation-induced hardening, is larger in Kapton H than in Kapton HA. Accordingly, the acoustic damping rate as measured by ISTS can be used to monitor *in situ* the extent of radiation-induced structural disorder and the resultant radiation-induced hardening of polyimide films. The thermal decay rate (see table 6) decreases comparably in Kapton H and HA upon irradiation. Since thermal diffusion occurs through acoustic phonon propagation, reduced thermal diffusivity is consistent with stronger acoustic damping and increased disorder that result from irradiation.

4.4 Conclusions

The results demonstrate general capabilities for *in-situ,* non-destructive evaluation (NDE) of radiation-induced material degradation. ISTS permits rapid, noninvasive determination of changes in viscoelastic and thermal properties caused by irradiation in a nuclear reactor. ISTS data for Kapton polyimide films are consistent with those of more conventional testing methods such as X-ray diffraction, dynamic viscoelasticity, and mechanical testing. ISTS measurements

of the type presented here are now routine and ISTS instruments based on a miniaturized optical apparatus are available commercially. The technique could be used for *in situ* evaluation of the changes that occur to nuclear reactor magnet insulation materials. The specific application demonstrated here is currently being researched for the International Thermonuclear Experimental Reactor (ITER). Kapton is used as a radiation insulation material in the particle accelerator at CERN and in other settings. There is a strong need for *in-situ* evaluation of radiation-induced damage from neutrons and other particles. ISTS measurements have been performed on ceramic [28] and metallic [29,30] materials as well as polymers, opening up the possibility that ISTS may also be useful for evaluation of other types of insulation materials such as alumina coatings or mica.

Chapter 5: Summary

The initial goal of this research project was to apply the already developed ISTS technique to new problems and in doing so, miniaturize the technique to make instrument development more feasible. In this thesis, the ability of ISTS to determine film thicknesses of metal films on silicon substrates has been proven and compared to a theoretical model as well as benchmarked against standard thickness techniques. This thesis has also demonstrated the potential for development of a compact, portable version of ISTS for use as a film thickness metrology instrument and other applications such as *in-situ,* non-destructive evaluation (NDE) of radiation-induced material degradation. Most effort has been focused on the technology and its application it to new material problems, however, contributions were made toward the development of the compact instrument. The product development aspect of the research will not be covered in this thesis as it is now fully in the hands of the company which will commercialize the ISTS technology. Appendix 1 shows pictures of the engineering prototype instrument and pictures and drawings of the beta-prototype instrument.

Previous development of the ISTS technique and the results of this research have laid the foundation for successful commercial development of ISTS as a thin film metrology instrument. Initially, the thrust is in the direction of metal film thickness determination for use in semiconductor manufacturing environments. Research continues in other areas of thin film research where ISTS may be a potentially valuable technique. For example, ion implantation in electronic materials is an area where metrology can add value by controlling dopant levels and depths. ISTS may be sensitive to the effects of ion implantation because ions disrupt the silicon lattice and should affect the mechanical properties. ISTS signal levels (as opposed to frequency measurements) have been found to correlate with uniformity of polysilicon deposition. Research is also beginning in the area of subsurface structure imaging.

Many other more focused thin film applications have been or are being investigated. ISTS measurements have been made on automotive paints and hard disk substrates. ISTS has been shown to be sensitive to gross delamination conditions and research continues in the hopes of being able to determine small differences in delamination conditions. There is a growing number of applications of thin films in areas of technology such as microelectronics, biomedicine and functional coatings. Many characterization techniques have potential for improving the level of control scientists and engineers have over thin films. ISTS is one such technique which can evaluate thin films and has the potential for improving manufacturing efficiency of thin films.

References

1. H.J. Maris, H. T. Grahn, and J. Tauc, Mat. Res. Soc. Symp. Proc. 142, 39 (1989).
2. T. Matikas, R. Crane, MRS Bulletin, 21 (10), 18 (1996).
3. Schneider, D., Scheibe, H.J., Schwarz, Th., Diamond and Related Materials, 2, 1396 (1993).
4. Rokhlin, S., Matikas, T., MRS Bulletin, 21 (10), 22 (1996).
5. Y. Yang, K.A. Nelson, and F. Adibi, J. Mater. Res. 10, 41 (1995).
6. J.K. Cocson, C.S. Hau, P.M. Lee, C.C. Poon, A.H. Zhong, J.A. Rogers, K.A. Nelson, J. Materials Science 30, 5960 (1995).
7. J.A. Rogers, L. Dhar, K.A. Nelson, Appl. Phys. Lett., 65 (3), 312 (1994).
8. J.A. Rogers, Y. Yang, K.A. Nelson, Appl. Phys. A, 58, 523 (1994).
9. J.A. Rogers and K.A. Nelson, IEEE Trans. Ultrasonics, Ferroelectrics, and Frequency Control 42 (4), 555 (1995).
10. J.A. Rogers and K.A. Nelson, J. Adhesion, 50, 1 (1995).
11. J.A. Rogers and K.A. Nelson, J. Polym. Sci. B, 34, 861 (1996).
12. A.R. Duggal, J.A. Rogers, K.A. Nelson, Appl. Phys. Lett. 60 (6), 692 (1992).
13. G.W. Farnell, E.L. Adler, Physical Acoustics, Principles and Methods, edited by W.P. Mason and R.N. Thurnston (Academic, New York, 1972), Vol. 9, p. 35.; H.J. Eichler, P. Gunter, D.W. Pohl, Laser-Induced Dynamic Gratings (Springer, Berlin, 1986).
14. J.A. Rogers and K.A. Nelson, J. Appl. Phys., 75, 1534 (1994).
15. A.R. Duggal, J.A. Rogers, K.A. Nelson, J. Appl. Phys., 72, 2823 (1992).
16. J.J. Estabil and M. Keefer, Solid State Tech., 38 (4), 71 (1995).
17. E. Irene, J. Woollam, MRS Bulletin, 20 (5), 24 (1995).
18. Hilfiker, Synowicki, Solid State Tech, 39 (10), 157 (1996).
19. J.S. Martens, S.M. Garrison, S.A. Sachtjen, Solid State Tech., 37 (12), 51 (1994).
20. P. Schmuki, M. Buchanan, B.F. Mason, G.I. Sproule, M.J. Graham, Appl. Phys. Lett., 68 (19), 2675 (1996).
21. Zayhowski, John, U.S. Patent 5,394,413, issue date Feb. 28, 1995.
22. Zayhowski, John, Optics Letters, 21 (8), 588 (1996).
23. Communication, Gary Bultman, Tencor Instruments, 1997.
24. CRC Handbook of Chemistry and Physics, Page E-41 (1971-72).
25. J.B. Schultz and R.P. Reed, Advances in Cryogenic Engineering, Plenum Press, New York, 1994, Vol. 40, 985.
26. Srinivasan, R. Hall, W. Loehle, W. Wilson, D. Albee, J. Appl. Phys. 78, 4881 (1995).
27. J. Megusar, J. Nuclear Materials, to be published, (1997).
28 Y. Yang, K.A. Nelson, and F. Adibi, J. Mater. Res. 10, 41 (1995).
29. R. Logan, A.A. Maznev, K.A. Nelson, J.A. Rogers, M. Banet, Mat. Res. Soc. Symp. Proc., to be published (1997).
30. A.A. Maznev, K.A. Nelson, T. Yagi, Thin Solid Films 290-291, 294 (1996).

Appendix 1

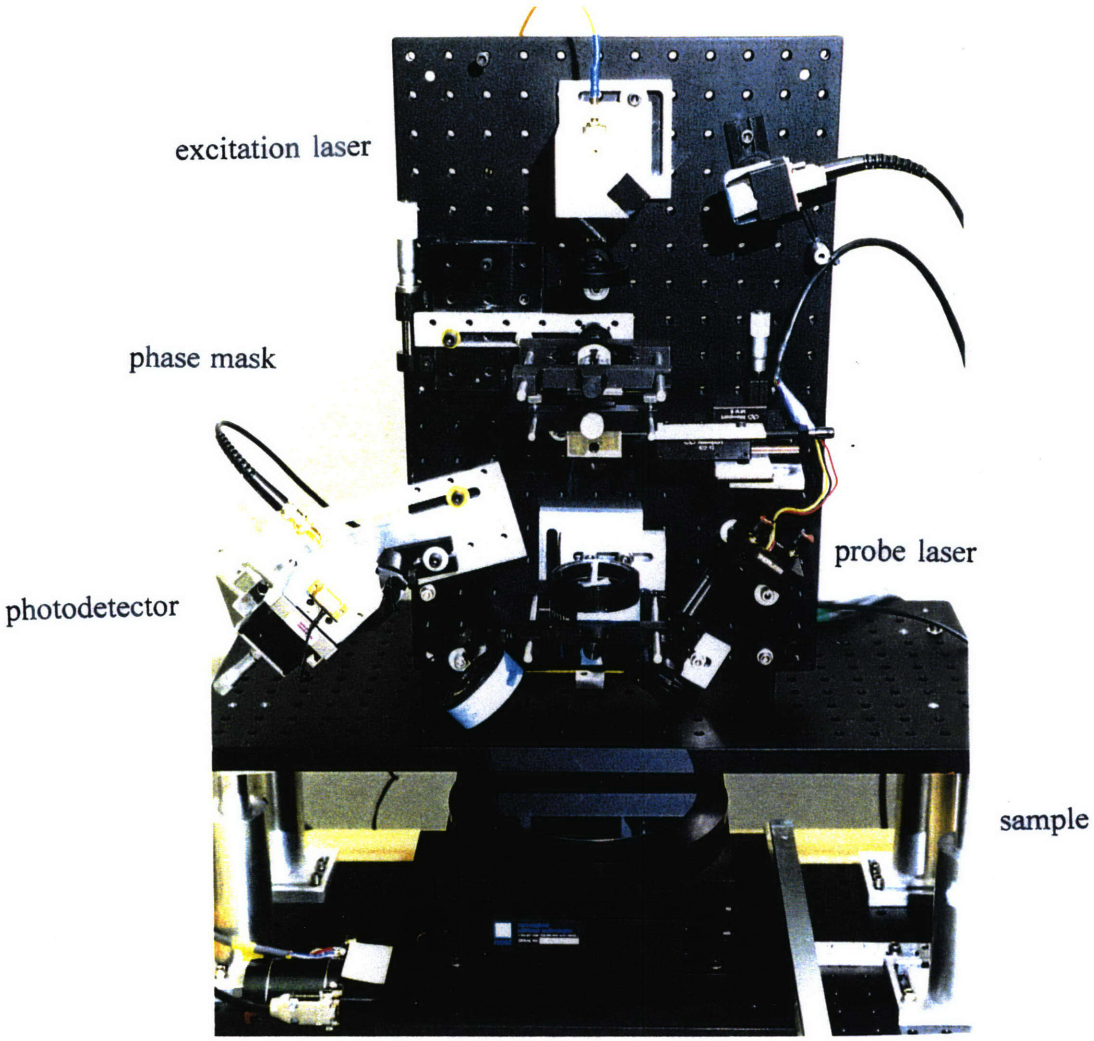

Photograph of breadboard prototype instrument.

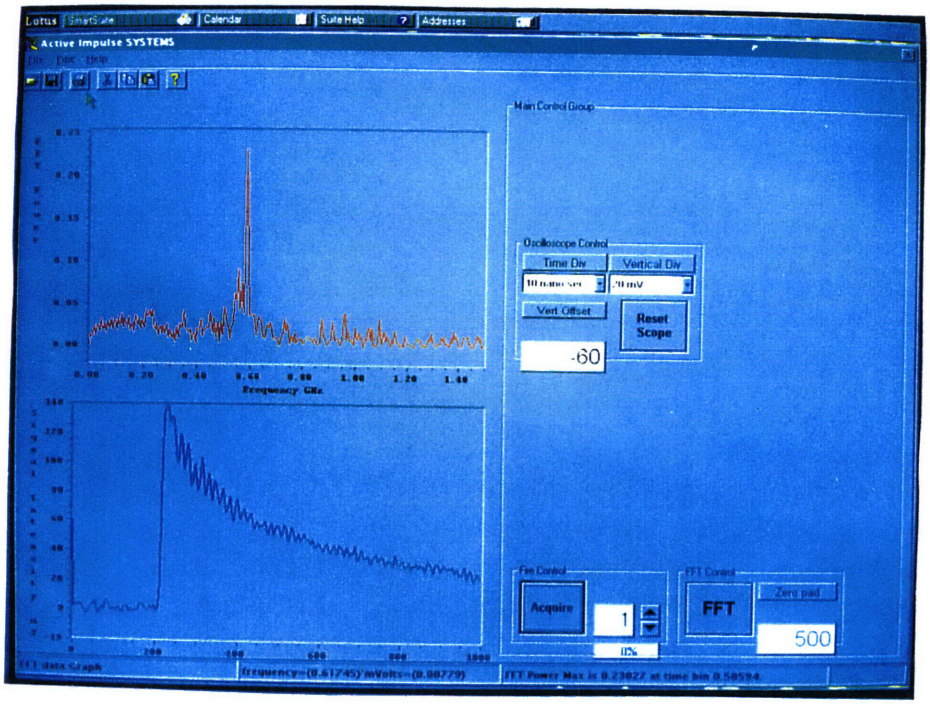

Photographs of complete system and user interface.

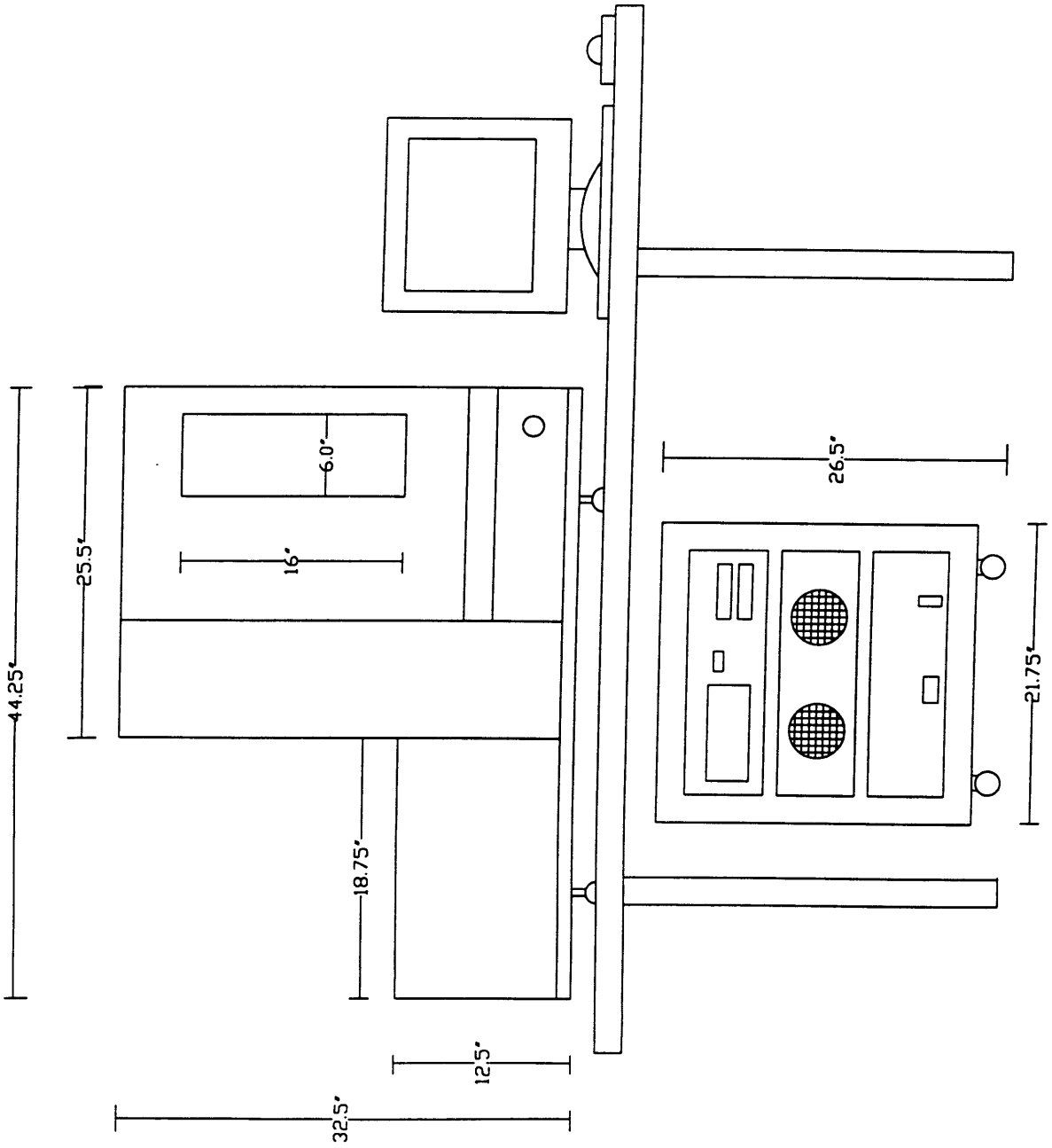

Side view schematic of beta-prototype.

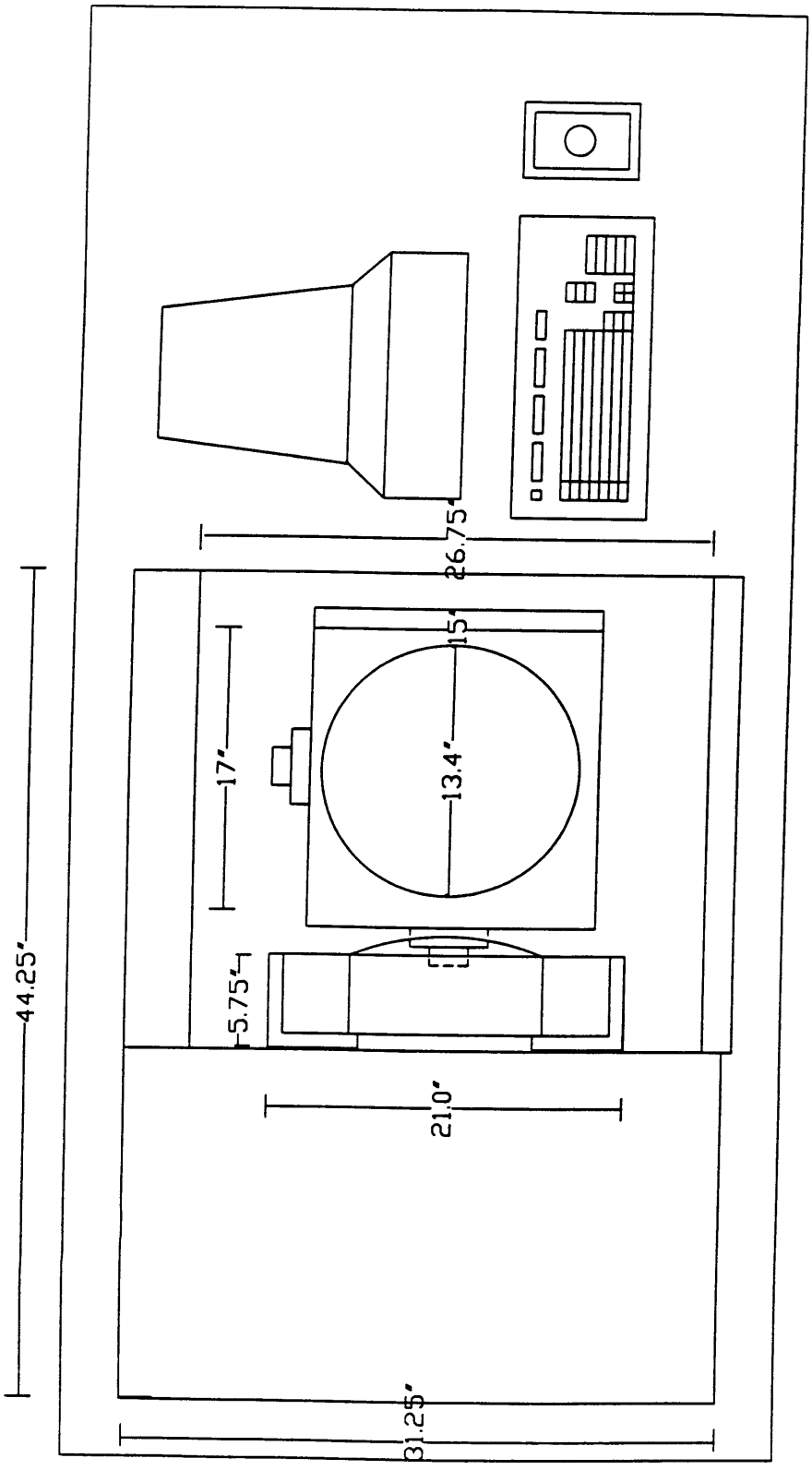

Top view schematic of beta-prototype.